

BASIC RESEARCH PAPER



Circular RNA *HIPK2* regulates astrocyte activation via cooperation of autophagy and ER stress by targeting *MIR124–2HG*

Rongrong Huang^{a,†}, Yuan Zhang^{a,†}, Bing Han^a, Ying Bai^a, Rongbin Zhou^b, Guangming Gan^c, Jie Chao^d, Gang Hu^e, and Honghong Yao^{a,f}

^aDepartment of Pharmacology, School of Medicine, Southeast University, Nanjing, Jiangsu, China; ^bInstitute of Immunology and the CAS Key Laboratory of Innate Immunity and Chronic Disease, School of Life Sciences and Medical Center, University of Science and Technology of China, Hefei, China; ^cDepartment of Genetics and Developmental Biology, School of Medicine, Southeast University, Nanjing, Jiangsu, China; ^dDepartment of Physiology, School of Medicine, Southeast University, Nanjing, Jiangsu, China; ^eJiangsu Key Laboratory of Neurodegeneration, Department of Pharmacology, Nanjing Medical University, Nanjing, Jiangsu, China; ^fInstitute of Life Sciences, Key Laboratory of Developmental Genes and Human Disease, Southeast University, Nanjing, Jiangsu, China

ABSTRACT

Circular RNAs are a subclass of noncoding RNAs in mammalian cells; however, whether these RNAs are involved in the regulation of astrocyte activation is largely unknown. Here, we have shown that the circular RNA *HIPK2* (*circHIPK2*) functions as an endogenous microRNA-124 (*MIR124–2HG*) sponge to sequester *MIR124–2HG* and inhibit its activity, resulting in increased sigma non-opioid intracellular receptor 1 (SIGMAR1/OPRS1) expression. Knockdown of *circHIPK2* expression significantly inhibited astrocyte activation via the regulation of autophagy and endoplasmic reticulum (ER) stress through the targeting of *MIR124–2HG* and SIGMAR1. These findings were confirmed in vivo in mouse models, as microinjection of a *circHIPK2* siRNA lentivirus into mouse hippocampi inhibited astrocyte activation induced by methamphetamine or lipopolysaccharide (LPS). These findings provide novel insights regarding the specific contribution of *circHIPK2* to astrocyte activation in the context of drug abuse as well as for the treatment of a broad range of neuroinflammatory disorders.

ARTICLE HISTORY

Received 9 September 2016
Revised 3 July 2017
Accepted 14 July 2017

KEYWORDS



astrocyte; autophagy; circular RNA *HIPK2*; endoplasmic reticulum; lipopolysaccharide; methamphetamine; *MIR124–2HG*; sigma non-opioid intracellular receptor 1


Introduction

Astrocytes, the most abundant cell type in the central nervous system (CNS), play critical roles in regulating and maintaining CNS homeostasis in normal physiological situations.^{1,2} In pathological conditions, astrocytes become activated and are characterized by abnormal morphology with reactive astrogliosis.^{3–7} Astrocyte activation plays a detrimental role in various neurological pathologies, including stroke,⁸ Parkinson disease,^{9,10} Alzheimer disease,^{11,12} and drug abuse.¹³ With respect to drug abuse, methamphetamine abuse is a major social and health concern. Astrocyte activation is associated with neuronal damage,^{14,15} as there is a close relationship between methamphetamine-induced degeneration of dopaminergic neurons in the striatum and concomitant reactive astrogliosis. Methamphetamine-induced neurotoxicity is associated with astrocyte activation in the striata of methamphetamine-treated mice and rats in vivo,^{16,17} and in vitro.^{18,19} Moreover, astrocyte activation contributes to the leakage of the blood-brain barrier (BBB) and facilitates the entry of molecules and immune cells into the CNS.²⁰ A detrimental role for astrocyte activation in the BBB damage is supported by a study showing that vascular endothelial growth factor from astrocytes increased the vascular permeability and CNS damage in acute inflammatory lesions.²¹

Together, evidence demonstrates that astrocyte activation plays a critical role in the recruitment of infiltrating immune cells into the CNS, with subsequent neuroinflammatory cascades resulting in brain tissue injury.

Methamphetamine is known to exhibit moderate affinity for SIGMAR1/OPRS1 (sigma non-opioid intracellular receptor 1), which is a unique drug-binding protein present in the CNS and periphery.^{22,23} Our previous study demonstrated that methamphetamine-mediated astrocyte activation involves the upregulation of SIGMAR1 expression through a positive feedback mechanism.¹³ Interestingly, our current study revealed that both methamphetamine and lipopolysaccharide (LPS) induce astrocyte activation via regulation of SIGMAR1 expression, suggesting that SIGMAR1 is a critical player in astrocyte activation. Although SIGMAR1 plays a crucial role in astrocyte activation, regulation of its expression by noncoding RNAs in astrocytes has not yet been explored. Computational algorithms, such as TargetScan, have been used to identify microRNAs (miRNAs) that target evolutionarily conserved sequences in the SIGMAR1-associated gene microRNA-124 (*MIR124–2HG*, the acronym formatting for humans is *MIR124–2HG* and for mice is *Mir124–2hg*, but we henceforth will use *MIR124–2HG* in both cases for the sake of simplicity),

CONTACT Honghong Yao  yaohh@seu.edu.cn  Department of Pharmacology, School of Medicine, Southeast University, Dingjiaqiao 87, Nanjing, Jiangsu 210009, China.

 Supplemental data for this article can be accessed on the [publisher's website](#).

[†]These two authors contributed to this work equally.

which is conserved among vertebrates and has been predicted to target *SIGMAR1*. It is the most abundant brain-specific miR that regulates neuronal differentiation during CNS development and adult neurogenesis.^{24–27} *MIR124–2HG* promotes microglial quiescence and suppresses experimental autoimmune encephalomyelitis by deactivating macrophages via the CEBPA/C/EBP- α -SPI1/PU.1 pathway.²⁸ Furthermore, a recent study indicated that *MIR124–2HG* inhibits microglial activation after focal cerebral ischemia.²⁹ However, whether *MIR124–2HG* regulates *SIGMAR1* expression and astrocyte activation remains to be elucidated.

Genome-wide bioinformatic analysis revealed that the circular RNA (circRNA) *HIPK2* (*circHIPK2*, the formatting for humans is *circHIPK2* and for mice is *circHipk2*, but we henceforth will use *circHIPK2* in both cases for the sake of simplicity), derived from exon 2 of the *HIPK2* gene, acts as a sponge for *MIR124–2HG*. CircRNAs, generated from back-spliced exons, have recently been identified as a naturally occurring family of noncoding RNAs that is highly represented in the eukaryotic transcriptome.³⁰ These endogenous RNAs are characterized by a stable structure and high tissue-specific expression.³¹ circRNAs are highly homologous to but generally more stable than their linear counterparts because they lack accessible ends and thus are resistant to exonucleases.³¹ While most of the circular RNAs reported so far have been exonic circular RNAs, a class of intron-containing exonic circRNAs is found predominantly in the nucleus,³² where they promote transcription of their parental genes. Several classes of noncoding RNAs have been shown to be involved in the regulation of physiological and pathophysiological processes including development and heart senescence, hypertrophy and failure, as well as cell growth.^{33–37} However, whether *circHIPK2* is involved in astrocyte activation remains largely unknown, and more extensive study is required.

In this study, we show that *circHIPK2* directly binds to *MIR124–2HG* and acts as an endogenous sponge for *MIR124–2HG* to inhibit its activity. Knockdown of *circHIPK2* expression significantly inhibited astrocyte activation via the regulation of autophagy and endoplasmic reticulum (ER) stress through the targeting of *MIR124–2HG*. These findings provide the first evidence that the *circHIPK2–MIR124–2HG* axis mediates a regulatory pathway critical for the regulation of astrocyte activation. Thus, specific blockage of *circHIPK2* could be a potential therapeutic target for inhibition of astrocyte activation in the context of drug abuse as well as the treatment of a broad range of neuroinflammatory disorders.

Results

MIR124–2HG participates in the regulation of *SIGMAR1*

Our previous study indicated that *SIGMAR1* upregulation is involved in methamphetamine-induced astrocyte activation. Interestingly, in the current study, we also demonstrated that LPS induced astrocyte activation via *SIGMAR1*. Treatment of astrocytes with LPS (100 ng/ml) significantly increased the expression of the astrocyte marker glial fibrillary acidic protein (GFAP) (Fig. S1A), with concomitant upregulation of *SIGMAR1* expression (Fig. S1B). These findings were further

confirmed in an in vivo experiment showing that LPS treatment increased the expression of both GFAP and *SIGMAR1* in wild-type (WT) mice and that the expression of these proteins was significantly inhibited in *sigmar1* knockout (KO) mice (Fig. S1C).

Given that *SIGMAR1* plays a critical role in astrocyte activation, we examined the mechanisms underlying *SIGMAR1* expression. MiRNAs are a class of small noncoding RNAs that act as negative regulators of gene expression. To determine whether *SIGMAR1* is regulated by miRs, we first predicted the presence of a consensus-binding site of *MIR124–2HG* in the 3'-untranslated region (3'-UTR) of *SIGMAR1* (the gene encoding *SIGMAR1*) using the TargetScan algorithm. As shown in Fig. 1A, *SIGMAR1* has a conserved *MIR124–2HG* binding site within its 3'-UTR in most species. Intriguingly, cotransfection of a *MIR124–2HG*-overexpressing vector and pmir-GLO plasmid with the *SIGMAR1* WT 3'-UTR resulted in the downregulation of luciferase activity, and this effect was reversed in HEK293T cells transfected with a mutated *SIGMAR1* 3'-UTR (Fig. 1B and Table 1A). Next, we aimed to determine whether methamphetamine mediates its effects via the induction of *MIR124–2HG* and to assess the kinetics of the methamphetamine response. Methamphetamine treatment of the human astrocyte cell line A172 and primary mouse astrocytes resulted in decreased *MIR124–2HG* expression (Fig. 1C and D). Interestingly and as expected, the methamphetamine-induced modulation of *MIR124–2HG* was inversely correlated with *SIGMAR1* expression (Fig. 1E and F). In line with this finding, *MIR124–2HG* decreased *SIGMAR1* expression, whereas *Anti-MIR124–2HG* increased its expression in both A172 cells (Fig. 1G) and primary mouse astrocytes (Fig. 1H) at the mRNA level. This finding was further confirmed at the protein level (Fig. 1I and J).

MIR124–2HG inhibits astrocyte activation by targeting *SIGMAR1* in vitro

Having determined that *MIR124–2HG* regulates *SIGMAR1* expression, we next examined the role of this miRNA in astrocyte activation. Cells were transduced with a lentivirus expressing a *MIR124–2HG* precursor, and GFAP expression was assessed. Transduction of cells with the *MIR124–2HG* precursor-expressing lentivirus resulted in significant inhibition of methamphetamine-induced astrocyte activation, as indicated by the GFAP expression levels in both A172 cells (Fig. 2A) and primary mouse astrocytes (Fig. 2B). Next, to determine whether the *MIR124–2HG*-mediated functional effects were specifically dependent on the upregulation of *SIGMAR1* expression, A172 cells were cotransduced with lentiviral vectors expressing *Anti-MIR124–2HG* and *SIGMAR1* siRNA. Transduction of cells with the *Anti-MIR124–2HG* lentivirus enhanced GFAP expression, and this effect was significantly inhibited in cells cotransduced with the lentiviral vectors expressing *Anti-MIR124–2HG* and *SIGMAR1* siRNA (Fig. 2C). Moreover, transduction of cells with the *Anti-MIR124–2HG* lentivirus resulted in enhanced GFAP expression (Fig. 2D), and this effect was inhibited in primary mouse astrocytes isolated from *sigmar1* KO mice. These rescue experiments were further confirmed in astrocytes treated with methamphetamine (Fig. S2A and B).

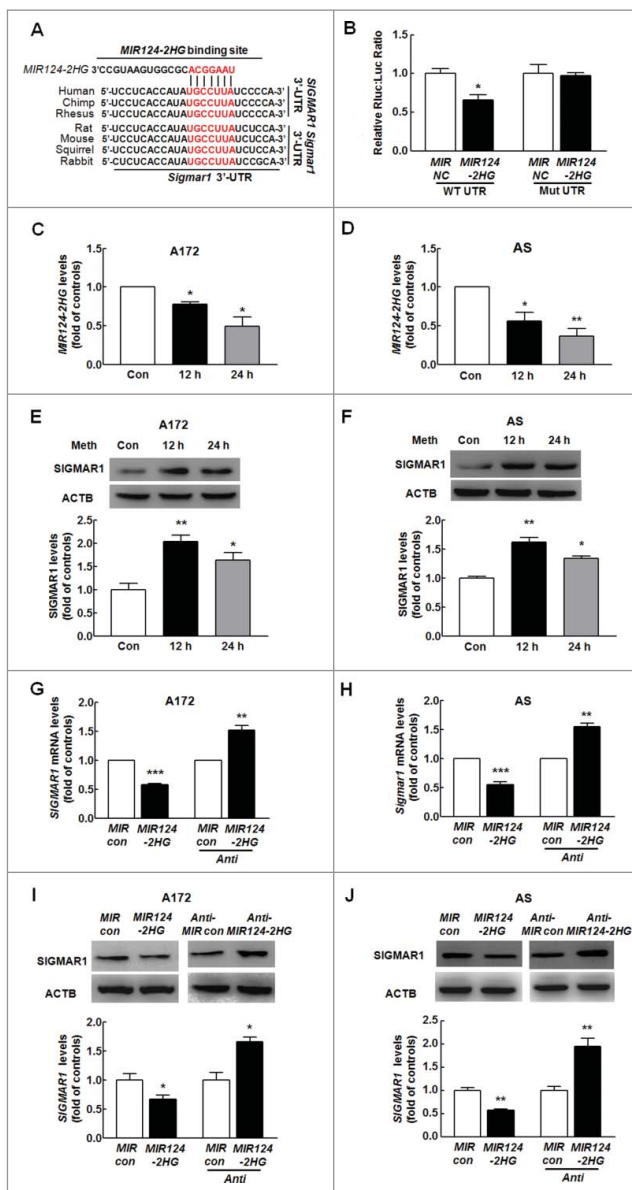


Figure 1. *MIR124-2HG* regulates *SIGMAR1* expression at the post-transcriptional level in astrocytes. (A) Putative *MIR124-2HG* binding sites in the 3'-UTR of *SIGMAR1* and *Sigmar1*. The potential complementary residues are shown in red. (B) Relative luciferase activity of wild-type and 3'-UTR mutant constructs of *SIGMAR1* cotransfected with a *MIR124-2HG* overexpression vector and pmiR-GLO plasmid. All data are presented as the means \pm SD of 3 individual experiments. * $P < 0.05$ vs. the *MIR control* cotransfected with the WT construct by one-way ANOVA, followed by the Holm-Sidak test. (C and D) Effect of methamphetamine on *MIR124-2HG* expression at the mRNA level in A172 cells (C) and primary mouse astrocytes (D) as determined by real-time PCR. Cells were incubated with methamphetamine (100 μ M) for 12 h and 24 h, followed by isolation of RNA for measurement of *MIR124-2HG* expression. All data are presented as the means \pm SD of 3 independent experiments. * $P < 0.05$ and ** $P < 0.01$ vs. the control group by the Student *t* test. (E and F) Effect of methamphetamine on *SIGMAR1* expression in A172 cells (E) and primary mouse astrocytes (F) as determined by western blotting. Cells were incubated with methamphetamine (100 μ M) for 12 h and 24 h, followed by measurement of *SIGMAR1* expression. Densitometric data of *SIGMAR1* expression using ImageJ are presented as the means \pm SD of 3 independent experiments. * $P < 0.05$ and ** $P < 0.01$ vs. the control group by the Student *t* test. (G and H) Cells were transfected with the *MIR control* or *MIR124-2HG* and *Anti-MIR control* or *Anti-MIR124-2HG* lentivirus for 24 h, and the mRNA expression of *SIGMAR1* was then measured by real-time PCR in A172 cells (G) and primary mouse astrocytes (H). (I and J) Cells were transfected with *MIR control* or *MIR124-2HG* and *Anti-MIR control* or *Anti-MIR124-2HG* lentivirus for 24 h, followed by measurement of *SIGMAR1* expression in A172 cells (I) and primary mouse astrocytes (J). Densitometric analysis of *SIGMAR1* expression using ImageJ is presented. All data are presented as the means \pm SD of 3 independent experiments. * $P < 0.05$, ** $P < 0.01$ and *** $P < 0.001$ vs. the *Mir control* or *Anti-MIR control* group by the Student *t* test. Meth, methamphetamine; AS, primary mouse astrocytes.

MIR124-2HG inhibits astrocyte activation by targeting *SIGMAR1* in vivo

Next, to determine whether the *Anti-MIR124-2HG*-mediated functional effects specifically depend on the upregulation of *SIGMAR1* expression, the hippocampi of WT and *sigmar1* KO mice were microinjected bilaterally with either an *Anti-MIR control*-RFP lentivirus or an *Anti-MIR124-2HG*-RFP lentivirus. It was important to first determine the efficacy of *Anti-MIR124-2HG*-RFP lentivirus transduction in vivo. As shown in Fig. 3A, *Anti-MIR control*-RFP-LV (lentivirus) or *Anti-MIR control*-LV-RFP or *Anti-MIR124-2HG*-LV-RFP expression was largely restricted to the hippocampus. As expected, increased *SIGMAR1* expression was observed on the *Anti-MIR124-2HG*-RFP-injected side compared with the *Anti-MIR control*-LV-RFP-injected side (Fig. 3B and C). Moreover, as shown in Fig. 3D and E, the *Anti-MIR124-2HG* lentivirus induced astrocyte activation, as indicated by the GFAP expression levels, in WT mice, and this effect was inhibited in the *sigmar1* KO mice injected with the lentiviral vector expressing *Anti-MIR124-2HG*. These findings thus support a role for *MIR124-2HG* in the regulation of methamphetamine-mediated astrocyte activation through the targeting of *SIGMAR1* in vivo. These results were further confirmed by immunostaining for GFAP, as shown in Fig. 3F and G. In WT mice, the *Anti-MIR124-2HG* lentivirus resulted in astrocyte activation in the hippocampus, as demonstrated by a significant increase in the relative integrated optical density (IOD) of GFAP immunoreactivity in astrocytes. However, these effects were inhibited in the *sigmar1* KO mice.

circHIPK2 binds *MIR124-2HG*

Having determined the role of *MIR124-2HG*-*SIGMAR1* axis in the astrocyte activation, we next get insight into the mechanisms of *MIR124-2HG* regulation. Since circRNAs act as competing endogenous RNA (ceRNA) sponges to interact with miRs and influence their activity, we sought to examine which circRNA can bind *MIR124-2HG*. Using a bioinformatics program, RNAhybrid (<http://bibiserv.techfak.uni-bielefeld.de/rna-hybrid>), we found that *circHIPK2* contains one *MIR124-2HG* target site (Fig. 4A). Consistent with the prediction, *circHIPK2* was expressed in primary mouse astrocytes as determined by *in*

Table 1. Succinct description of mutated or modified molecules.

Original molecules	Mutated or modified molecules	Succinct descriptions
A. pmiR-RB- <i>SIGMAR1</i> 3'-UTR vector	pmiR-RB- <i>SIGMAR1</i> 3'-UTR mutant vector	A vector containing mutated <i>SIGMAR1</i> 3'-UTR that does not target <i>MIR124-2HG</i>
B. <i>circHIPK2</i> probe	biotin-labeled <i>circHIPK2</i> probe	A single strand DNA probe capable of combining <i>circHIPK2</i>
C. <i>MIR124-2HG</i>	3'-end biotinylated <i>MIR124-2HG</i>	A 3'-end biotinylated microRNA mimic
D. <i>MIR124-2HG</i>	<i>MIR124-2HG</i> Δ	A mutated sequence that does not target the 3'-UTR of <i>SIGMAR1</i>
E. <i>MIR124-2HG</i> probe	digoxigenin-labeled <i>MIR124-2HG</i> probe	A single strand DNA probe capable of combining <i>MIR124-2HG</i>

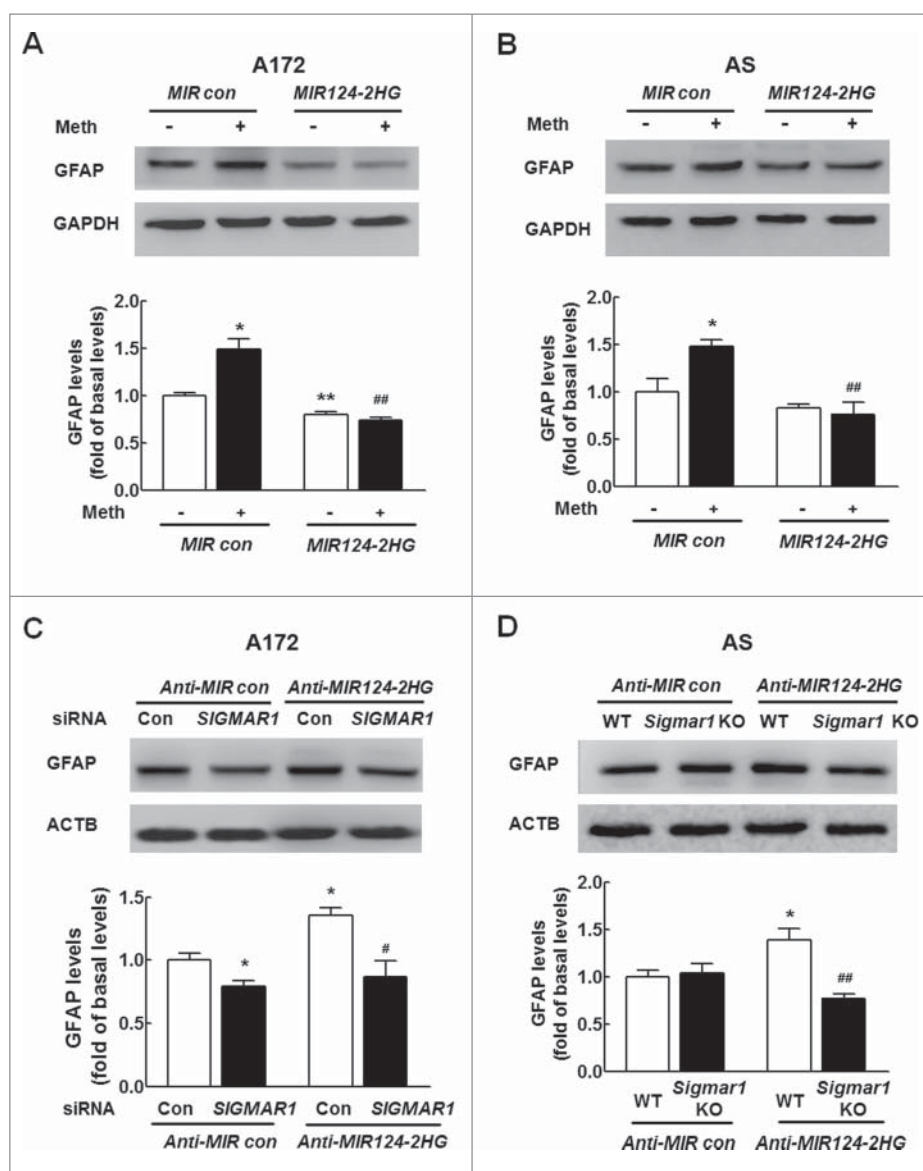


Figure 2. *MIR124-2HG* inhibits astrocyte activation by targeting *SIGMAR1* in vitro. (A and B) Transduction of cells with *MIR124-2HG* attenuated methamphetamine-induced astrocyte activation in A172 cells (A) and primary mouse astrocytes (B), as determined by western blotting for GFAP expression. Cells were transduced with a *MIR124-2HG* lentivirus for 24 h, treated with methamphetamine (100 μ M) for 12 h followed by measurement of GFAP expression. AS, primary mouse astrocytes. Densitometric data of GFAP expression using ImageJ are presented as the means \pm SD of 3 independent experiments. * P < 0.05 and ** P < 0.01 vs. the *MIR control* group; ## P < 0.01 vs. the methamphetamine-treated *MIR control* group by one-way ANOVA, followed by the Holm-Sidak test. (C) Transfection of A172 cells with *SIGMAR1* siRNA significantly inhibited *Anti-MIR124-2HG*-induced astrocyte activation, as determined by western blotting. Densitometric data of GFAP expression using ImageJ are presented as the means \pm SD of 3 independent experiments. * P < 0.05 vs. the *Anti-MIR control* group; # P < 0.05 vs. the *Anti-MIR124-2HG* cotransfected with siRNA control, by one-way ANOVA, followed by the Holm-Sidak test. (D) Transduction of *Anti-MIR124-2HG* induced astrocyte activation in primary mouse astrocytes isolated from WT mice but not in *sigmar1* KO mice, as determined by western blotting. Densitometric data of GFAP expression using ImageJ are presented as the means \pm SD of 3 independent experiments. * P < 0.05 vs. *Anti-MIR control* transfected into primary mouse astrocytes isolated from WT mice; ## P < 0.01 vs. *Anti-MIR124-2HG* transduced into primary mouse astrocytes isolated from WT mice by one-way ANOVA, followed by the Holm-Sidak test. Meth, methamphetamine; AS, primary mouse astrocytes; *MIR124*, *MIR124-2HG*.

situ hybridization analysis using a *circHIPK2*-specific probe (Fig. 4B and Table. 1B). We then assessed whether *circHIPK2* is involved in astrocyte activation induced by different stimuli by qRT-PCR using divergent primers (Fig. 4C). Treatment of astrocytes with methamphetamine significantly increased *circHIPK2* expression in both A172 cells and primary mouse astrocytes (Fig. 4D). Furthermore, we applied a biotin-coupled *MIR124-2HG* mimic (Table 1C) to test whether *MIR124-2HG* was able to pull down *circHIPK2*. We observed enrichment of *circHIPK2* in the *MIR124-2HG*-captured fraction compared with that observed following the introduction of mutations that disrupt base pairing between *circHIPK2* and *MIR124-2HG*

(Fig. 4E). Furthermore, double *in situ* hybridization indicated that there was colocalization of *circHIPK2* and *MIR124-2HG* in primary mouse astrocytes (Fig. 4F).

Knockdown of *circHIPK2* expression inhibits astrocyte activation by targeting *MIR124-2HG* in vitro

To study the effects of *circHIPK2* on *SIGMAR1* expression and astrocyte activation, astrocytes were transfected with *circHIPK2* siRNA. As shown in Fig. S3, *circHIPK2* siRNA caused a decrease in *circHIPK2* expression compared with the control siRNA, as determined by real-time PCR. We

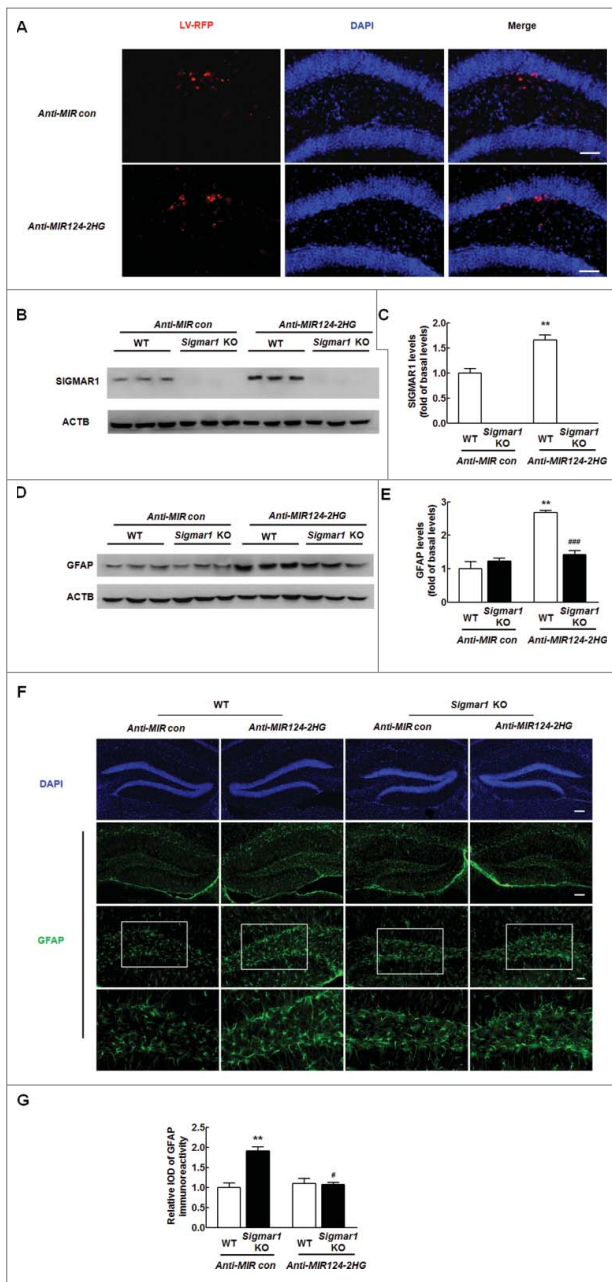


Figure 3. *MIR124-2HG* inhibits astrocyte activation by targeting *SIGMAR1* in vitro. (A) Representative images of C57BL/6 mice microinjected with either *Anti-MIR control-RFP* or *Anti-MIR124-2HG-RFP* lentivirus into the hippocampus. Scale bar: 20 μm . The hippocampi of mice were microinjected bilaterally with an *Anti-MIR-RFP* lentivirus ($2 \mu\text{l}$ of 10^9 viral genomes μl^{-1}); the mice were killed 2 weeks after microinjection, and RFP expression was measured. (B and C) *Anti-MIR124-2HG* lentivirus injection successfully increased *SIGMAR1* expression, as determined by western blotting. Two wk after microinjection, the mice were killed, and *SIGMAR1* expression was measured (B). Densitometric analysis of *SIGMAR1* expression using ImageJ (C). (D and E) *GFAP* expression in the hippocampus was determined in WT and *sigmar1* KO mice. WT and *sigmar1* KO mice were microinjected with either an *Anti-MIR control-RFP* or *Anti-MIR124-2HG-RFP* lentivirus. Two wk after microinjection, the mice were killed, and *GFAP* expression was determined by western blotting (D). Densitometric analysis of *GFAP* expression using ImageJ (E). $N = 6$ animals/group. ** $P < 0.01$ vs. the *Anti-MIR control*-microinjected WT group; and ### $P < 0.001$ vs. the *Anti-MIR124-2HG-RFP*-microinjected WT group by one-way ANOVA, followed by the Holm-Sidak test. (F) Representative images of *GFAP* immunostaining in the hippocampi of the mice, as described above. Scale bars: 50 μm (upper panel), 50 μm (middle panel) and 20 μm (lower panel). The bottom panels depict outlines of portions of the astrocytes from the corresponding images above. (G) Quantification of *GFAP* immunofluorescence intensity using ImageJ software. IOD, integrated optical density. $N = 6$ animals/group. ** $P < 0.01$ vs. the *Anti-MIR control*-microinjected WT group; # $P < 0.05$ vs. the *Anti-MIR124-2HG-RFP*-microinjected WT group by one-way ANOVA, followed by the Holm-Sidak test.

further assessed the effect of *circHIPK2* on methamphetamine-induced astrocyte activation. As shown in Fig. 5A, transfection of cells with *circHIPK2* siRNA significantly inhibited methamphetamine-induced astrocyte activation, as determined by western blotting (WB) for *GFAP* expression. We also examined the effect of *circHIPK2* on *SIGMAR1* expression. The results showed that knockdown of *circHIPK2* significantly inhibited the methamphetamine-induced increase in *SIGMAR1* expression. Notably, transfection of cells with *circHIPK2* siRNA resulted in decreased *SIGMAR1* expression (Fig. 5B). Next, to further verify that *MIR124-2HG* is a mediator of *circHIPK2*, A172 astrocytes were cotransfected with *Anti-MIR124-2HG* and *circHIPK2*. Knockdown of *circHIPK2* attenuated the inductive effects of *Anti-MIR124-2HG* on *SIGMAR1* expression (Fig. 5C) and astrocyte activation, as indicated by the *GFAP* expression levels (Fig. 5D). To claim that these individually observed effects of *MIR124-2HG* or *circHIPK2* on astrocyte activation were induced by methamphetamine, these rescue experiments were performed under methamphetamine treatment. Consistent with the findings, knockdown of *circHIPK2* significantly inhibited the expression of *SIGMAR1* and activation of astrocytes induced by *Anti-MIR124-2HG* in primary mouse astrocytes treated with methamphetamine as shown in Fig. S4A and B. These results indicate that *circHIPK2* acts as an endogenous *MIR124-2HG* sponge to regulate *SIGMAR1* expression and astrocyte activation.

Knockdown of *circHIPK2* expression inhibits astrocyte activation in vivo

Having demonstrated that *circHIPK2*, involved in regulating *SIGMAR1* expression, plays a critical role in astrocyte activation, we sought to validate the role of *circHIPK2* in vivo by microinjecting a *circHIPK2* siRNA lentivirus into the hippocampi of C57BL/6 mice. The hippocampi of C57BL/6 mice were microinjected bilaterally with either a *circ* siRNA control-GFP lentivirus or a *circHIPK2* siRNA-GFP lentivirus and monitored for astrocyte activation in response to methamphetamine. However, it was important to first determine the efficacy of *circHIPK2* siRNA-GFP lentivirus transduction in vivo. As shown in Fig. 6A, *GFP* expression was largely restricted to the hippocampus. As expected, decreased *circHIPK2* expression was observed on the *circHIPK2* siRNA-injected side compared with the *circ* siRNA control-GFP lentivirus-injected side (Fig. 6B). Two wk after the administration of the lentivirus, the mice were treated with methamphetamine (30 mg/kg), and *GFAP* expression in the hippocampus was assessed. As shown in Fig. 6C and D, methamphetamine treatment increased *GFAP* and *SIGMAR1* expression compared with saline treatment, and these effects were significantly attenuated by *circHIPK2* siRNA microinjection. Similar to the methamphetamine treatment, *circHIPK2* siRNA microinjection also significantly inhibited the LPS-induced increase in *GFAP* expression, as shown in Fig. 6E and F. These results were further confirmed by immunostaining (Fig. 6G and H).

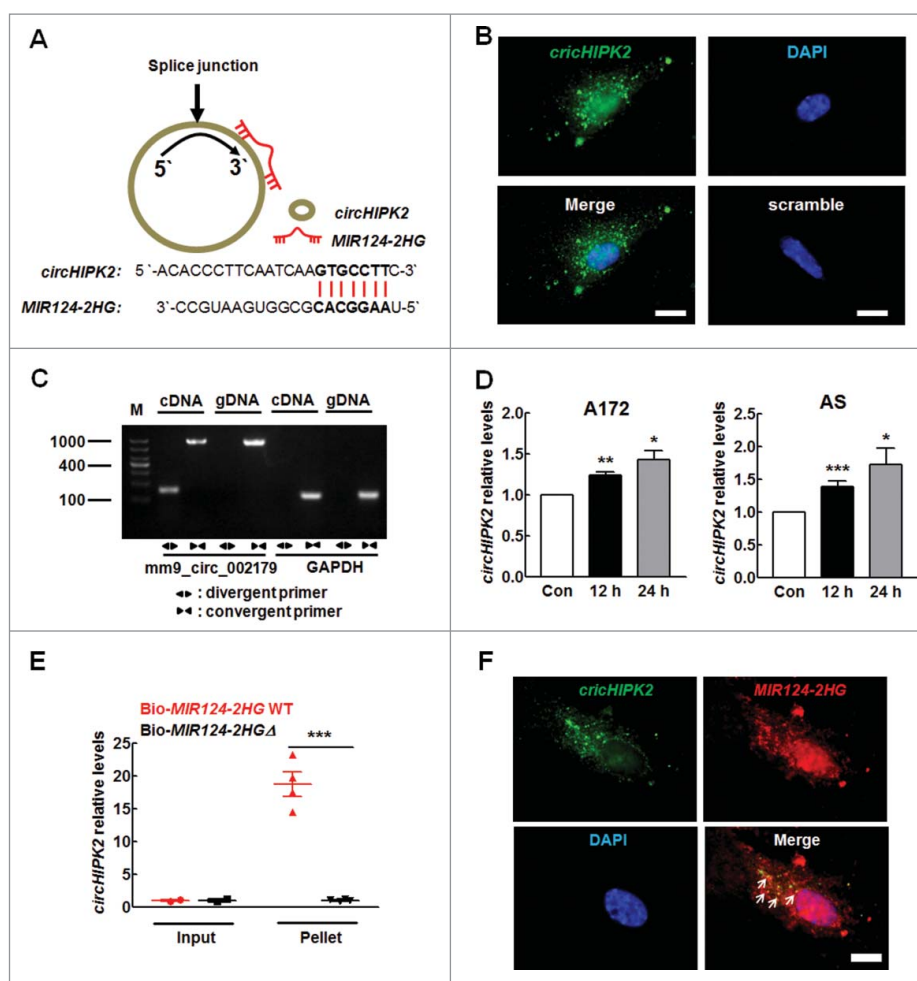


Figure 4. *circHIPK2* binds *MIR124-2HG*. (A) *circHIPK2* contains one site complementary to *MIR124-2HG*, as analyzed using the RNAhybrid bioinformatics program (upper panel). A biotin-coupled *MIR124-2HG* mutant is shown in the lower panel. (B) Fluorescence *in situ* hybridization of *circHIPK2* in primary mouse astrocytes. Green, *circHIPK2*; Blue, DAPI. Scale bars: 5 μ m. (C) Divergent primers amplified circRNAs in cDNA but not in genomic DNA (gDNA). GAPDH, linear control. (D) Methamphetamine increased the *circHIPK2* levels in A172 cells (left panel) and primary mouse astrocytes (right panel), as determined by real-time PCR. All data are presented as the means \pm SD of 3 independent experiments. * $P < 0.05$, ** $P < 0.01$ and *** $P < 0.001$ vs. the control group by the Student *t* test. (E) Biotinylated WT *MIR124-2HG* (Bio-*MIR124-2HG* WT) or its mutant (Bio-*MIR124-2HG*Δ) was transfected into HEK293T cells. After streptavidin capture, the *circHIPK2* and *GAPDH* mRNA levels were quantified by real-time PCR, and the relative immunoprecipitate (IP)/input ratios were plotted. All data are presented as the mean \pm SD of 3 independent experiments. *** $P < 0.001$ vs. the Bio-124-WT group by the Student *t* test. (F) Fluorescence *in situ* hybridization of *circHIPK2* and *MIR124-2HG* in primary mouse astrocytes. Green, *circHIPK2*; Red, *MIR124-2HG*; Blue, DAPI. Scale bars: 5 μ m. Arrows indicate the colocalization of *circHIPK2* and *MIR124-2HG*. Meth, methamphetamine; AS, primary mouse astrocytes.

Knockdown of *circHIPK2* expression inhibits astrocyte autophagy by targeting *MIR124-2HG*

Having determined that *circHIPK2* is involved in methamphetamine-induced astrocyte activation, we next assessed the underlying mechanisms. First, we examined the effect of methamphetamine on MAP1LC3B/LC3B-II expression in astrocytes. As shown in Fig. 7A, methamphetamine treatment of A172 cells increased the expression of ATG5 and BECN1/Beclin 1 and induced the production of MAP1LC3B-II, which is a cleaved MAP1LC3B-phosphatidylethanolamine conjugate and a general autophagosomal marker.³⁸ These findings were further confirmed in primary mouse astrocytes (Fig. 7B). During the process of autophagy, SQSTM1/p62 acts as a receptor protein that links MAP1LC3B with ubiquitin moieties on misfolded proteins. Therefore, autophagy mediates the clearance of SQSTM1 along with ubiquitinated proteins. Consistently, SQSTM1 expression was downregulated by methamphetamine treatment in both A172 cells (Fig. 7A) and primary mouse

astrocytes (Fig. 7B). This effect was also confirmed by immunofluorescence staining, which showed that methamphetamine treatment resulted in an increased number of vacuoles, as indicated by the endogenous MAP1LC3B-II expression levels (Fig. 7C).

Autophagy is a dynamic process of protein degradation characterized by the formation of double-membraned cytoplasmic vesicles.³⁹ Structural analysis via electron microscopy allows for the visualization of autophagy, characterized by the massive accumulation of autophagic vacuoles (autophagosomes) and autolysosomes in the cytoplasm. As shown in Fig. 7D, methamphetamine treatment resulted in the accumulation of numerous autolysosomes (arrow) and double-membraned autophagic vacuoles (arrowhead) in A172 cells.

Autophagic flux was further monitored in A172 astrocytes that were transduced with a tandem fluorescent-mRFP-GFP-MAP1LC3B-adenovirus, a specific marker of autophagosome formation that relies on the differences in GFP and RFP

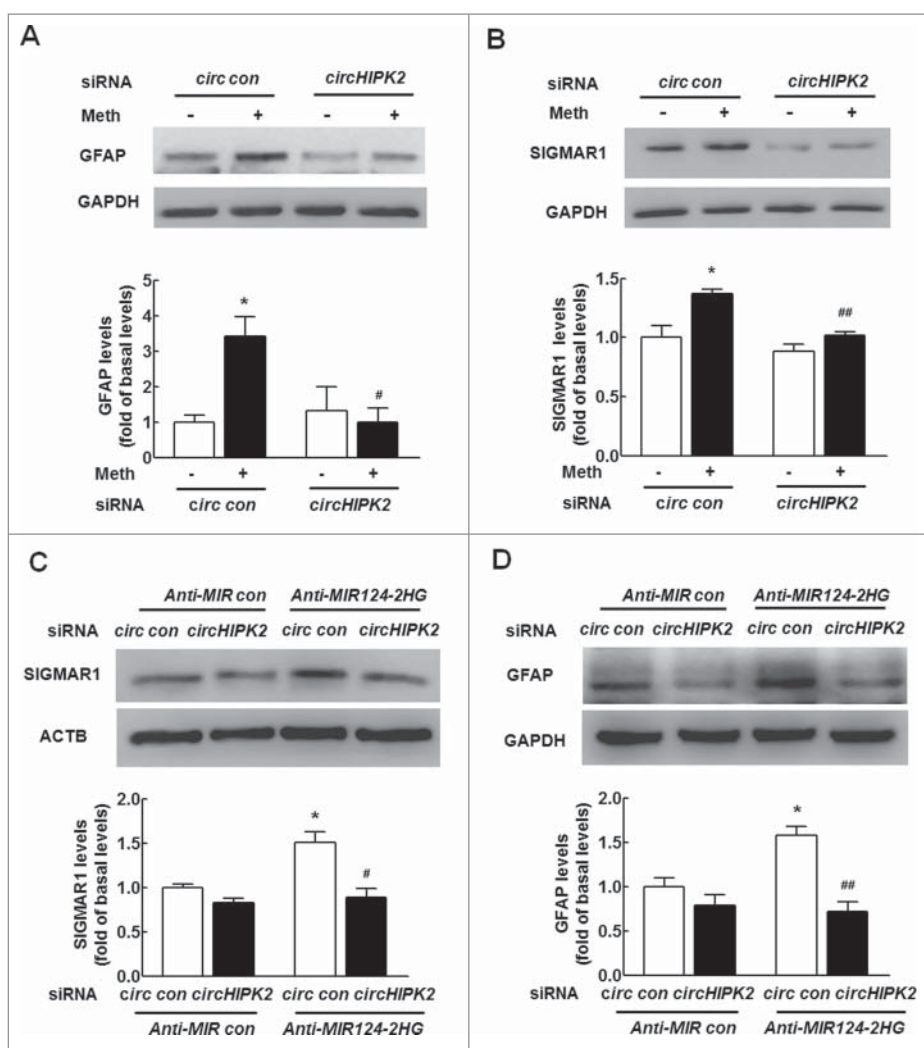


Figure 5. Knockdown of *circHIPK2* expression inhibits astrocyte activation by targeting *MIR124-2HG* in vitro. (A) Transfection of cells with *circHIPK2* siRNA attenuated methamphetamine-induced astrocyte activation, as determined by western blotting for GFAP expression. Cells were transfected with *circHIPK2* siRNA for 24 h and were then treated with methamphetamine (100 μ M) for 12 h, and GFAP expression was measured. (B) Transfection of cells with *circHIPK2* siRNA attenuated the methamphetamine-induced increase in SIGMAR1 expression, as determined by western blotting. Densitometric data of GFAP and SIGMAR1 expression using ImageJ are presented as the means \pm SD of 3 independent experiments. * $P < 0.05$ vs. the siRNA control group; # $P < 0.05$ and ## $P < 0.01$ vs. the methamphetamine-treated siRNA control group by one-way ANOVA, followed by the Holm-Sidak test. (C and D) Transduction of A172 cells with *Anti-MIR124-2HG* significantly inhibited *circHIPK2* siRNA-induced SIGMAR1 expression (C) and astrocyte activation (D), as determined by western blotting. Densitometric data of GFAP and SIGMAR1 expression using ImageJ are presented as the means \pm SD of 3 independent experiments. * $P < 0.05$ vs. the *Anti-MIR* control cotransduced with siRNA control; # $P < 0.05$ and ## $P < 0.01$ vs. the *Anti-MIR124-2HG* cotransduced with siRNA control, by one-way ANOVA, followed by the Holm-Sidak test. Meth, methamphetamine.

fluorescence under acidic conditions. GFP fluorescence is sensitive to the acidic conditions of the lysosome lumen, while RFP is relatively stable under acidic conditions. Thus, the colocalization of GFP and RFP signals (yellow dots) indicates the lack of fusion of phagophores or autophagosomes with lysosomes, whereas RFP-only signals (red puncta) indicate the presence of autolysosomes. As shown in Fig. 7E, methamphetamine treatment significantly increased the number of yellow dots per cell, with a concomitant greater increase in RFP-only MAP1LC3B dots in primary mouse microglia transduced with tandem fluorescent-tagged nRFP-GFP-MAP1LC3B.

Next, we elucidated the effect of *circHIPK2* on astrocyte autophagy. As shown in Fig. 8A, transfection of cells with *circHIPK2* siRNA significantly inhibited methamphetamine-induced astrocyte autophagy, as determined by WB for MAP1LC3B-II expression. Having determined that *MIR124-*

2HG regulates astrocyte activation, we next examined its role in astrocyte autophagy. Transduction of cells with a *MIR124-2HG* precursor-expressing lentivirus significantly inhibited methamphetamine-induced astrocyte autophagy, as indicated by the MAP1LC3B-II expression levels, in both A172 cells (Fig. 8B) and primary mouse astrocytes (Fig. 8C). Next, to determine whether the *MIR124-2HG*-mediated functional effects are specifically dependent on the upregulation of SIGMAR1 expression, A172 cells were cotransduced with lentiviral vectors expressing *Anti-MIR124-2HG* and SIGMAR1 siRNA. Transduction of cells with the *Anti-MIR124-2HG* lentivirus enhanced GFAP expression, and this effect was significantly inhibited in cells cotransduced with the lentiviral vectors expressing *Anti-MIR124-2HG* and SIGMAR1 siRNA (Fig. 8D). Moreover, transduction of cells with the *Anti-MIR124-2HG* lentivirus resulted in enhanced MAP1LC3B-II expression (Fig. 8E), and this effect was inhibited in primary mouse

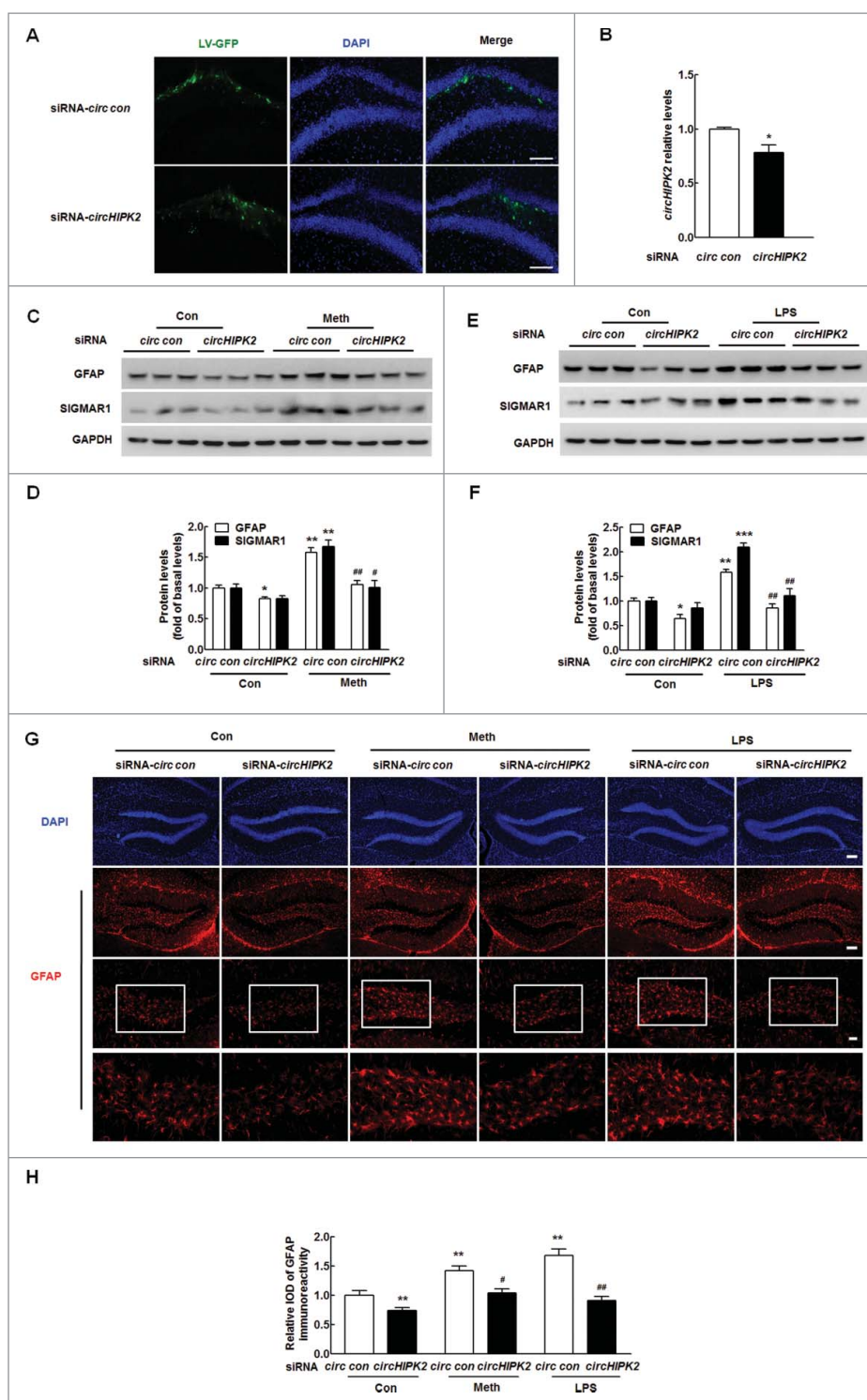


Figure 6. Knockdown of *circHIPK2* expression inhibits astrocyte activation. (A) Representative images of hippocampi of C57BL/6 mice microinjected with *circ* siRNA-GFP lentivirus. Scale bar: 100 μ m. The hippocampi of mice were microinjected bilaterally with either *circ* siRNA control-GFP or *circHIPK2* siRNA-GFP lentivirus (2μ l of 10^9 viral genomes μ l $^{-1}$); the mice were killed 2 wk after microinjection, and GFP expression was measured. (B) *circHIPK2* siRNA lentivirus injection successfully decreased *circHIPK2* expression, as determined by real-time PCR. Two wk after microinjection, the mice were killed, and *circHIPK2* expression was measured. $N = 6$ animals/group. * $P < 0.05$ vs. the *circ* siRNA control group by the Student t test. (C and D) Microinjection of the *circHIPK2* siRNA lentivirus into the hippocampus inhibited methamphetamine-induced astrocyte activation (C). Densitometric data of GFAP and SIGMAR1 expression using ImageJ (D) are shown *MIR124-2HG*. (E and F) Microinjection of the *circHIPK2* siRNA lentivirus into the hippocampus inhibited astrocyte activation induced by LPS (E). Densitometric data of GFAP and SIGMAR1 expression using ImageJ (F) are shown. (G) Representative images of GFAP immunostaining in the hippocampi of mice treated with methamphetamine or LPS, as described above. Scale bars: 50 μ m (upper panel), 50 μ m (middle panel) and 20 μ m (lower panel). The bottom panels depict outlines of segmented astrocytes from the corresponding images above. (H) Quantification of GFAP immunofluorescence intensity using ImageJ software. IOD, integrated optical density. Two wk after microinjection, the mice were treated with methamphetamine (i.p., 30 mg/kg) for 24 h or with LPS (i.p., 20 mg/kg) for 4 h. $N = 6$ animals/group. * $P < 0.05$, ** $P < 0.01$ and *** $P < 0.001$ vs. the saline-treated *circ* siRNA control group; # $P < 0.05$ and ## $P < 0.01$ vs. the methamphetamine- or LPS-treated *circ* siRNA control group by one-way ANOVA, followed by the Holm-Sidak test. Meth, methamphetamine.

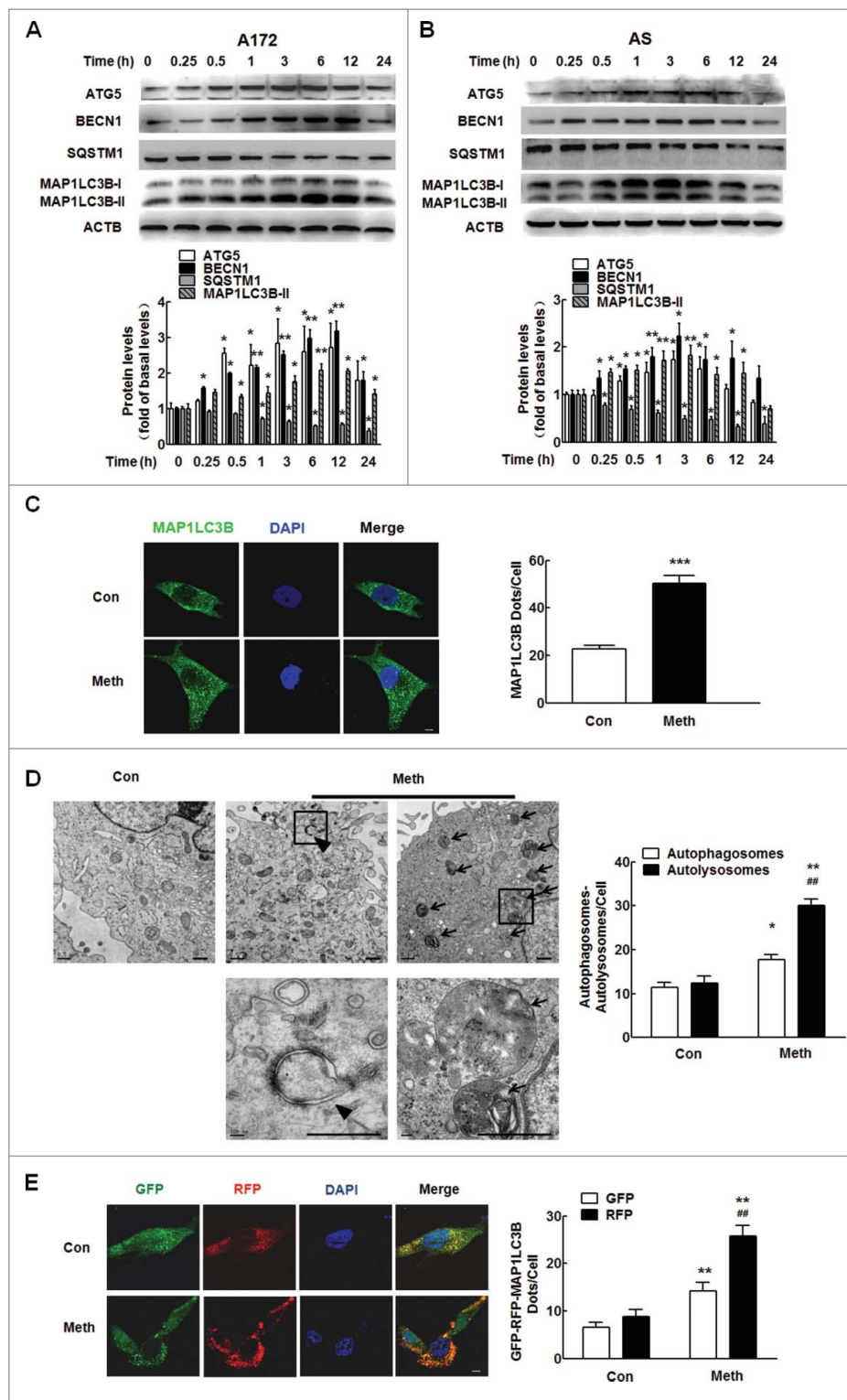


Figure 7. Methamphetamine induces astrocyte autophagy. (A and B) The expression of ATG5, BECN1, MAP1LC3B-II and SQSTM1 in A172 cells (A) and primary mouse astrocytes (B) induced by methamphetamine. Cells were treated with methamphetamine (100 μ M) for 0.25 h, 0.5 h, 1 h, 3 h, 6 h, 12 h and 24 h. Densitometric data of ATG5, BECN1, MAP1LC3B-II and SQSTM1 expression using ImageJ are presented as the means \pm SD of 3 independent experiments. * P < 0.05 and ** P < 0.01 vs. the control group by the Student t test. (C) Effect of methamphetamine on the formation of MAP1LC3B puncta. Cells were treated with methamphetamine (100 μ M) for another 12 h. MAP1LC3B puncta were then analyzed by confocal microscopy. Scale bar: 20 μ m. All data are presented as the means \pm SD of 3 independent experiments. *** P < 0.001 vs. the control group by the Student t test. (D) Transmission electron microscopic imaging showing autolysosomes (arrows) and autophagosomes with double-membraned autophagic vacuoles (arrowheads) in primary microglial cells (left panel) and quantification of autolysosomes and autophagosomes (right panel) in primary microglial cells treated with methamphetamine (100 μ M) for 12 h. Scale bar: 200 nm. (E) A172 cells were infected with an RFP-GFP-MAP1LC3B adenovirus and were then treated with 100 μ M methamphetamine for 12 h. Effects of methamphetamine on RFP- and GFP-MAP1LC3B puncta (left panel). Scale bar: 5 μ m. The numbers of RFP- and GFP-MAP1LC3B puncta per cell were counted, and the results are shown in the right panel. The numbers of puncta per cell are presented as the means \pm SD of 3 independent experiments. * P < 0.05 and ** P < 0.01 vs. the control group; ## P < 0.01 vs. the methamphetamine-treated group by one-way ANOVA, followed by the Holm-Sidak test. Meth, methamphetamine; AS, primary mouse astrocytes.

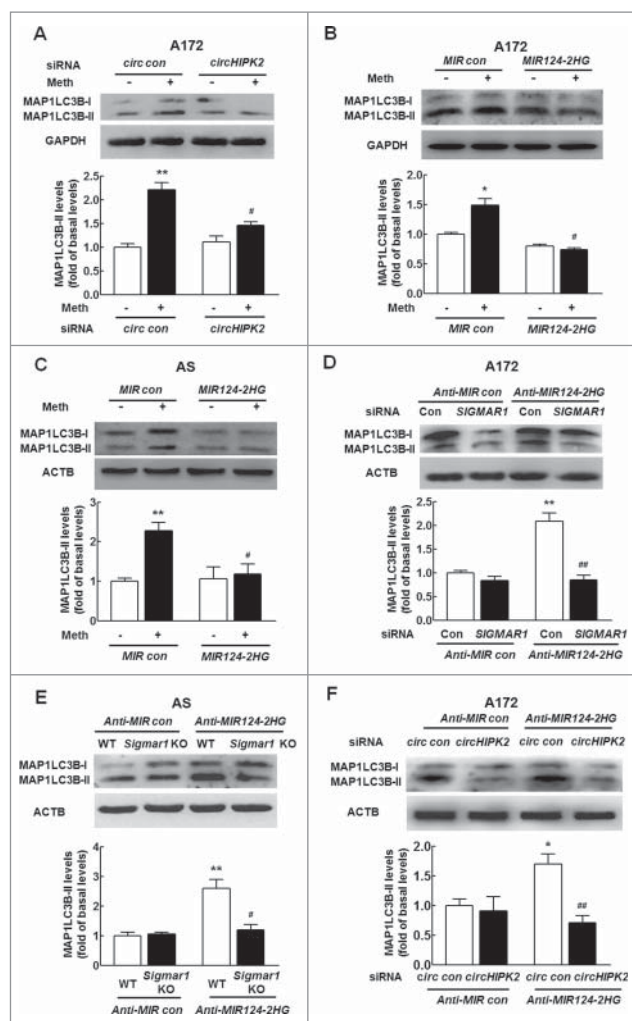


Figure 8. Knockdown of *circHIPK2* expression inhibits astrocyte autophagy by targeting *MIR124-2HG*. (A) Transfection of cells with *circHIPK2* siRNA attenuated methamphetamine-induced astrocyte autophagy, as determined by western blotting for MAP1LC3B-II expression. Cells were transfected with *circHIPK2* siRNA for 24 h and were then treated with methamphetamine (100 μ M) for 12 h, followed by measurement of MAP1LC3B-II expression using ImageJ are presented as the means \pm SD of 3 independent experiments. $**P < 0.01$ vs. the siRNA control group; $\#P < 0.05$ vs. the methamphetamine-treated siRNA control group by one-way ANOVA, followed by the Holm-Sidak test. (B and C) Transduction of cells with *MIR124-2HG* attenuated methamphetamine-induced astrocyte autophagy in A172 cells (B) and primary mouse astrocytes (C), as determined by western blotting for MAP1LC3B-II expression. Densitometric data of MAP1LC3B-II expression using ImageJ are presented as the means \pm SD of 3 independent experiments. $*P < 0.05$ and $**P < 0.01$ vs. the *MIR control* group; $\#P < 0.05$ vs. the methamphetamine-treated *MIR control* group by one-way ANOVA, followed by the Holm-Sidak test. (D) Transfection of A172 cells with *SIGMAR1* siRNA significantly inhibited *Anti-MIR124-2HG*-induced astrocyte autophagy, as determined by western blotting. Densitometric data of MAP1LC3B-II expression using ImageJ are presented as the means \pm SD of 3 independent experiments. $**P < 0.01$ vs. the *Anti-MIR control* group; $\#P < 0.01$ vs. the *Anti-MIR124-2HG* cotransduced with siRNA control, by one-way ANOVA, followed by the Holm-Sidak test. (E) Transduction of *Anti-MIR124-2HG* induced astrocyte activation in primary mouse astrocytes isolated from WT mice but not in *sigmar1* KO mice, as determined by western blotting. Densitometric data of MAP1LC3B-II expression using ImageJ are presented as the means \pm SD of 3 independent experiments. $**P < 0.01$ vs. *Anti-MIR control* transduced into primary mouse astrocytes isolated from WT mice; $\#P < 0.05$ vs. *Anti-MIR124-2HG* transduced into primary mouse astrocytes isolated from WT mice by one-way ANOVA, followed by the Holm-Sidak test. (F) Transfection of A172 cells with *Anti-MIR124-2HG* significantly inhibited the *circHIPK2* siRNA-induced increase in MAP1LC3B-II expression, as determined by western blotting. Densitometric data of MAP1LC3B-II expression using ImageJ are presented as the means \pm SD of 3 independent experiments. $*P < 0.05$ vs. *Anti-MIR control* cotransduced with siRNA control; $\#P < 0.01$ vs. the *Anti-MIR124-2HG* cotransduced with siRNA control, by one-way ANOVA, followed by the Holm-Sidak test. Meth, methamphetamine; AS, primary mouse astrocytes.

astrocytes isolated from *sigmar1* KO mice. In addition, knock-down of *circHIPK2* expression significantly attenuated the inductive effect of *Anti-MIR124-2HG* on astrocyte autophagy (Fig. 8F). These rescue experiments were further confirmed in astrocytes treated with methamphetamine as shown in Fig. S5A-C. These results indicate that *circHIPK2* acts as an endogenous *MIR124-2HG* sponge to regulate astrocyte autophagy.

Knockdown of *circHIPK2* expression inhibits ER stress in astrocytes by targeting *MIR124-2HG*

Having determined that *circHIPK2* is involved in methamphetamine-induced astrocyte activation and autophagy, we next investigated the role of *circHIPK2* in ER stress in astrocytes. First, we examined the effect of methamphetamine on ER stress in astrocytes. As shown in Fig. S6, methamphetamine treatment of A172 astrocytes increased the expression of EIF2AK3/PERK, EIF2S1/EIF-2 α , DDIT3/CHOP, ERN1/IRE1 and ATF6.

Next, we assessed the effect of *circHIPK2* on ER stress in astrocytes. As shown in Fig. 9A, transfection of astrocytes with *circHIPK2* siRNA significantly inhibited methamphetamine-induced ER stress, as demonstrated by WB for DDIT3 expression. Having determined that *MIR124-2HG* regulates astrocyte activation and autophagy, we next examined its role in ER stress in astrocytes. Transduction of cells with a *MIR124-2HG* precursor-expressing lentivirus significantly inhibited the methamphetamine-induced ER stress associated with astrocyte autophagy, as indicated by the DDIT3 expression levels, in both A172 cells (Fig. 9B) and primary mouse astrocytes (Fig. 9C). Next, to determine whether the *MIR124-2HG*-mediated functional effects are specifically dependent on the upregulation of *SIGMAR1* expression, A172 cells were cotransduced with lentiviral vectors expressing *Anti-MIR124-2HG* and *SIGMAR1* siRNA. Transduction of cells with the *Anti-MIR124-2HG* lentivirus enhanced DDIT3 expression, and this effect was significantly inhibited in cells cotransduced with the lentiviral vectors expressing *Anti-MIR124-2HG* and *SIGMAR1* siRNA (Fig. 9D). Moreover, transduction of cells with the *Anti-MIR124-2HG* lentivirus resulted in enhanced DDIT3 expression (Fig. 9E), and this effect was inhibited in primary mouse astrocytes isolated from *sigmar1* KO mice. Next, we further assessed whether *MIR124-2HG* is a mediator of *circHIPK2*. A172 astrocytes were cotransfected with the *Anti-MIR124-2HG* lentivirus and *circHIPK2* siRNA, and DDIT3 expression was measured. As shown in Fig. 9F, knockdown of *circHIPK2* expression significantly counteracted the inductive effect of *Anti-MIR124-2HG* on ER stress in astrocytes. These rescue experiments were further confirmed in astrocytes treated with methamphetamine, as shown in Fig. S7A to C. These results indicate that *circHIPK2* acts as an endogenous *MIR124-2HG* sponge to regulate ER stress in astrocytes.

Distinct roles of autophagy and ER stress in methamphetamine-induced astrocyte activation

Having determined that methamphetamine induces astrocyte activation, we next sought to examine the roles of autophagy

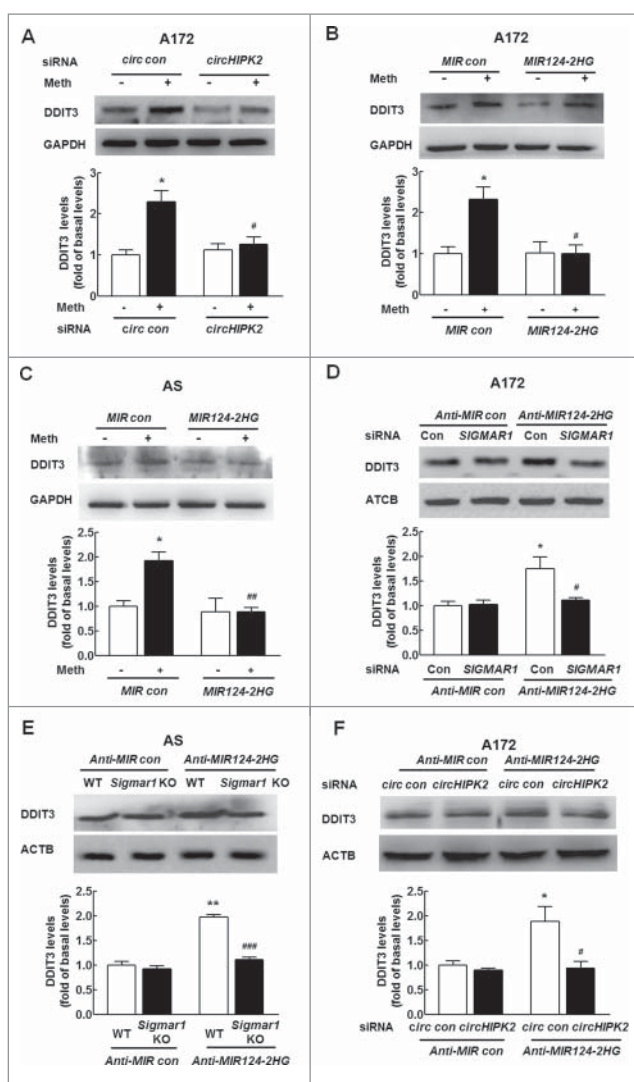


Figure 9. Knockdown of *circHIPK2* expression inhibits ER stress in astrocytes by targeting *MIR124-2HG*. (A) Transfection of cells with *circHIPK2* siRNA attenuated methamphetamine-induced ER stress in astrocytes, as determined by western blotting for DDIT3 expression. Densitometric data of DDIT3 expression using ImageJ are presented as the means \pm SD of 3 independent experiments. * $P < 0.05$ vs. the siRNA control group; and # $P < 0.05$ vs. the methamphetamine-treated siRNA control group by one-way ANOVA, followed by the Holm-Sidak test. (B and C) Transduction of cells with *MIR124-2HG* attenuated methamphetamine-induced ER stress in A172 cells (B) and primary mouse astrocytes (C), as determined by western blotting for DDIT3 expression. Densitometric data of DDIT3 expression using ImageJ are presented as the means \pm SD of 3 independent experiments. * $P < 0.05$ vs. the *MIR* control group; # $P < 0.05$ and ### $P < 0.01$ vs. the methamphetamine-treated *MIR* control group by one-way ANOVA, followed by the Holm-Sidak test. (D) Transfection of A172 cells with *SIGMAR1* siRNA significantly inhibited *Anti-MIR124-2HG*-induced ER stress in astrocytes, as determined by western blotting. Densitometric data of DDIT3 expression using ImageJ are presented as the means \pm SD of 3 independent experiments. * $P < 0.05$ vs. *Anti-MIR* control cotransduced with siRNA control; # $P < 0.05$ vs. *Anti-MIR124-2HG* cotransduced with siRNA control, by one-way ANOVA, followed by the Holm-Sidak test. (E) Transduction of *Anti-MIR124-2HG* induced ER stress in primary mouse astrocytes isolated from WT mice but not in *sigmar1* KO mice, as determined by western blotting. Densitometric data of DDIT3 expression using ImageJ are presented as the means \pm SD of 3 independent experiments. ** $P < 0.01$ vs. *Anti-MIR* control transduced into primary mouse astrocytes isolated from WT mice; ### $P < 0.001$ vs. *Anti-MIR124-2HG* transduced into primary mouse astrocytes isolated from WT mice by one-way ANOVA, followed by the Holm-Sidak test. (F) Transduction of A172 cells with *Anti-MIR124-2HG* significantly inhibited the *circHIPK2* siRNA-induced increase in DDIT3 expression, as determined by western blotting. Densitometric data of DDIT3 expression using ImageJ are presented as the means \pm SD of 3 independent experiments. * $P < 0.05$ vs. *Anti-MIR* control cotransduced with siRNA control; # $P < 0.05$ vs. *Anti-MIR124-2HG* cotransduced with siRNA control, by one-way ANOVA, followed by the Holm-Sidak test. Meth, methamphetamine; AS, primary mouse astrocytes.

and ER stress in this process. Pretreatment of cells with an ER stress inhibitor, salubrinal, significantly inhibited methamphetamine-induced astrocyte activation (Fig. 10A and B), suggesting that ER stress enhances activation of these cells. Salubrinal acts as a phosphatase inhibitor and increases EIF2S1 phosphorylation, leading to a global decrease in translation and a subsequent reduction in ER stress. Moreover, both A172 cells and primary mouse astrocytes were treated with an autophagy inhibitor, 3-methyladenine (3-MA), which is a PtdIns3K inhibitor that prevents autophagy at an early stage of autophagosome formation. As shown in Fig. 10C and D, pretreatment of cells with 3-MA enhanced methamphetamine-induced GFAP expression in both A172 astrocytes (Fig. 10C) and primary mouse astrocytes (Fig. 10D). However, pretreatment of cells with an autophagy inducer, rapamycin significantly lessened methamphetamine-induced astrocyte activation in both A172 astrocytes (Fig. 10E) and primary mouse astrocytes (Fig. 10F). This finding was further confirmed in vivo, as rapamycin pretreatment significantly inhibited activation of astrocytes induced by methamphetamine, with concomitant enhancement of autophagy (Fig. S8). These findings suggest that autophagy inhibits astrocyte activation, while the inhibition of autophagy results in enhanced astrocyte activation.

Interplay between autophagy and ER stress induced by methamphetamine

Having determined that methamphetamine induces autophagy and ER stress in astrocytes, further study was undertaken to elucidate the role of ER stress in the autophagy induced by methamphetamine using the ER stress inhibitor salubrinal. As shown in Fig. 11A and B, pretreatment of cells with salubrinal resulted in abrogation of the increased autophagy induced by methamphetamine as evidenced by decreased expression of MAP1LC3B-II, thereby confirming that ER stress response is upstream of autophagy in methamphetamine-treated astrocytes. We next assessed the effect of autophagy on the ER stress response. Pretreatment of cells with the autophagy inducer rapamycin resulted in abrogation of the increased ER stress induced by methamphetamine as evidenced by decreased expression of DDIT3 in both A172 cells (Fig. 11C) and primary mouse astrocytes (Fig. 11D). Consistent with this finding, pretreatment of cells with the autophagy inhibitor 3-MA further enhanced the increased ER stress in both A172 cells (Fig. 11E) and primary mouse astrocytes (Fig. 11F), suggesting an interplay between autophagy and the ER stress response in astrocytes induced by methamphetamine.

Discussion

Our study provides new insights into the function of *circHIPK2*, which was found to significantly inhibit astrocyte activation via the regulation of autophagy and ER stress via the targeting of *MIR124-2HG* and subsequent targeting of *MIR124-2HG*-*SIGMAR1* (Fig. 12). These findings provide the first evidence that the *circHIPK2*-*MIR124-2HG* axis mediates a regulatory pathway critical for the regulation of astrocyte activation. Specific blockage of *circHIPK2* could be envisioned as a potential therapeutic target for the inhibition of astrocyte

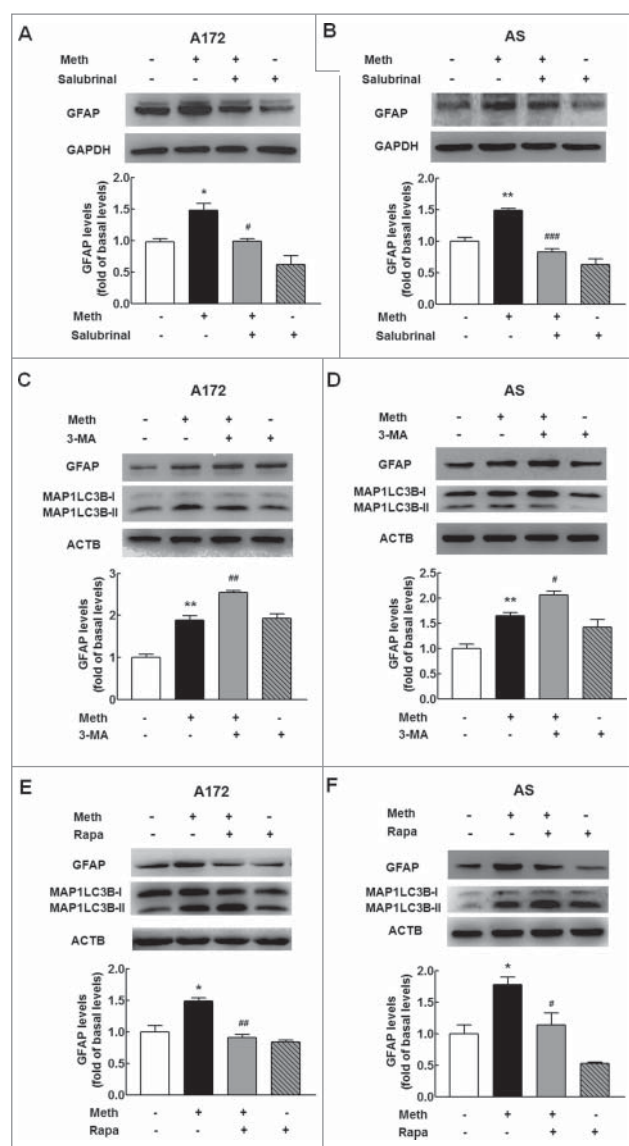


Figure 10. Distinct roles of autophagy and ER stress in methamphetamine-induced astrocyte activation. (A and B) Pretreatment of cells with an ER stress inhibitor, salubrinal, significantly inhibited methamphetamine-induced astrocyte activation in A172 cells (A) and primary mouse astrocytes (B). Cells were pretreated with salubrinal (20 μ M) for 1 h and were then treated with methamphetamine (100 μ M) for 12 h. (C and D) Pretreatment of cells with an autophagy inhibitor, 3-MA (3 mM), enhanced methamphetamine-induced astrocyte activation in A172 cells (C) and primary mouse astrocytes (D). Cells were pretreated with 3-MA (3 mM) for 1 h and were then treated with methamphetamine (100 μ M) for 3 h. (E and F) Pretreatment of cells with an autophagy inducer, rapamycin, attenuated methamphetamine-induced astrocyte activation in A172 cells (E) and primary mouse astrocytes (F). Cells were pretreated with rapamycin (0.1 μ M) for 1 h and were then treated with methamphetamine (100 μ M) for 12 h. All densitometric data of GFAP expression using ImageJ are presented as the means \pm SD of 3 independent experiments. * P < 0.05 and ** P < 0.01 vs. the control group; # P < 0.05, ## P < 0.01 and ### P < 0.001 vs. the methamphetamine-treated group by one-way ANOVA, followed by the Holm-Sidak test. Meth, methamphetamine; AS, primary mouse astrocytes; 3-MA, 3-methyladenine; Rapa, rapamycin.

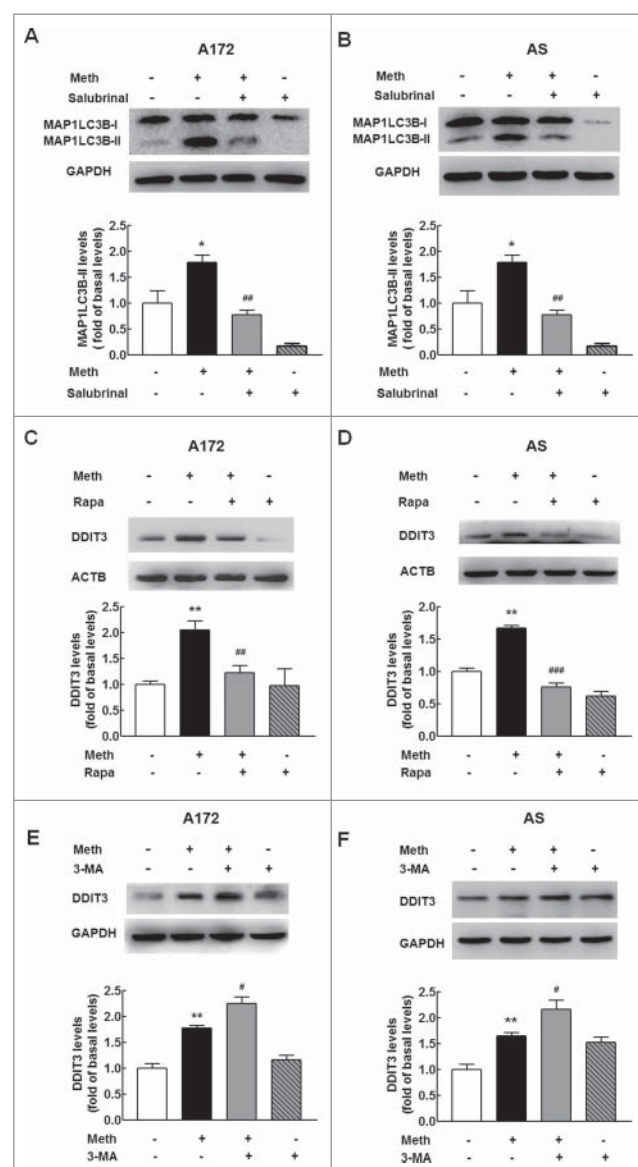


Figure 11. Interplay between autophagy and ER stress induced by methamphetamine. (A and B) Pretreatment of cells with an ER stress inhibitor, salubrinal, significantly inhibited methamphetamine-induced astrocyte autophagy in A172 cells (A) and primary mouse astrocytes (B). Cells were pretreated with salubrinal (20 μ M) for 1 h and were then treated with methamphetamine (100 μ M) for 12 h. (C and D) Pretreatment of cells with an autophagy inducer, rapamycin, attenuated methamphetamine-induced astrocyte ER stress in A172 cells (C) and primary mouse astrocytes (D). Cells were pretreated with rapamycin (0.1 μ M) for 1 h and were then treated with methamphetamine (100 μ M) for 12 h. (E and F) Pretreatment of cells with an autophagy inhibitor, 3-MA (3 mM), enhanced methamphetamine-induced astrocyte ER stress in A172 cells (E) and primary mouse astrocytes (F). Cells were pretreated with 3-MA (3 mM) for 1 h and were then treated with methamphetamine (100 μ M) for 3 h. All densitometric data of MAP1LC3B-II and DDIT3 expression using ImageJ are presented as the means \pm SD of 3 independent experiments. * P < 0.05 and ** P < 0.01 vs. the control group; # P < 0.05, ## P < 0.01 and ### P < 0.001 vs. the methamphetamine-treated group by one-way ANOVA, followed by the Holm-Sidak test. Meth, methamphetamine; AS, primary mouse astrocytes; 3-MA, 3-methyladenine; Rapa, rapamycin.

activation in the context of drug abuse as well as in the treatment of a broad range of neuroinflammatory disorders.

Astrocyte activity may exacerbate inflammatory reactions and neuronal tissue damage or promote immune suppression and tissue repair depending on the timing and context.²⁰ However, clinical and experimental findings have indicated that astrocyte activation is critically involved in the pathogenesis of

neurotoxicity induced by methamphetamine,⁴⁰ strongly suggesting that the inflammatory status might critically determine the outcome and prognosis of neuronal tissue injury. Strategies aimed at mitigation of astrocyte activation have been shown to have therapeutic potential in experimental models of neuroinflammation induced by methamphetamine. Thus, researchers have recently focused on developing anti-inflammatory

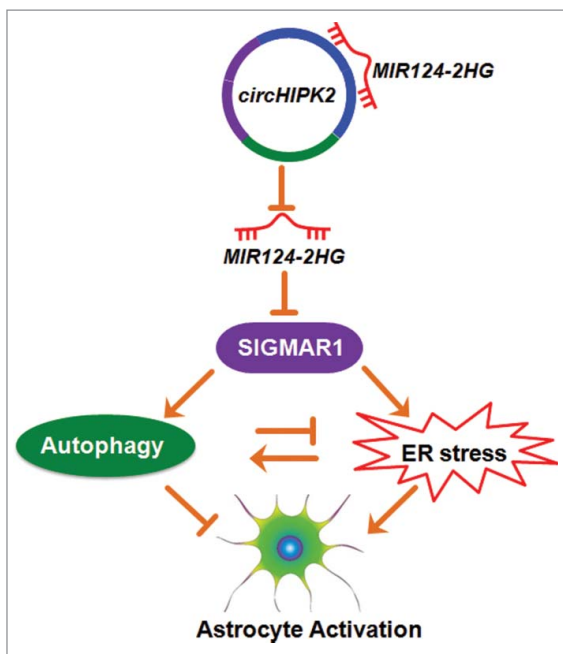


Figure 12. Role of *circHIPK2* in astrocyte activation. *circHIPK2*, identified as a ceRNA, functions as an endogenous *MIR124-2HG* sponge to sequester *MIR124-2HG* and inhibit its activity, resulting in increased *SIGMAR1* expression and consequent astrocyte activation via the interplay between autophagy and endoplasmic reticulum stress.

strategies for the treatment of astrocyte activation induced by methamphetamine. For example, our previous studies and other studies indicate that inhibition of *SIGMAR1* significantly lessens astrocyte activation.^{17,41} In this study, we explored molecular players with pivotal roles in astrocyte activation.

Accumulating evidence indicates that circRNAs are not simply the by-products of mis-splicing or splicing errors; in fact, they have important functions in development and heart senescence, hypertrophy and failure, as well as cell growth.³³⁻³⁶ Despite the biological importance of circRNAs, it has not yet been clarified whether they are involved in the regulation of astrocyte activation in the brain. Our present study revealed a novel function of *circHIPK2* in the regulation of astrocyte activation via the interplay between autophagy and ER stress. A better understanding of the role of this circRNA in astrocyte activation may facilitate the identification of a novel therapeutic target for the treatment or control of related diseases.

A previous study showed that circRNAs may act as endogenous sponges that interact with miRs and regulate the expression of miRNA target genes. In addition, a recent study demonstrates that the circRNA HRCR acts as a *MIR223* sponge to regulate cardiac hypertrophy and heart failure.³⁷ Consistent with previous studies, our current study revealed that *circHIPK2* acts as a *MIR124-2HG* sponge to regulate *SIGMAR1* expression and astrocyte activation. To improve knockdown efficiency and minimize off-target effects, we further constructed a second *circHIPK2* siRNA-GFP lentivirus (*circHIPK2* siRNA2) in addition to the first *circHIPK2* siRNA-GFP lentivirus (*circHIPK2* siRNA1) microinjected in Fig. 6B. Transduction of primary mouse astrocytes with these 2 different *circHIPK2* siRNA-GFP lentivirus constructs decreased the expression of *circHIPK2* by 41% for *circHIPK2* siRNA1 versus 40% for *circHIPK2* siRNA2 (Fig. S9A), which are higher than that in A172

cells transfected with human-specific *circHIPK2* siRNA (Fig. S3). Furthermore, we also performed *circHIPK2* loss-of-function experiments. Knockdown of *circHIPK2* expression significantly inhibited activation (Fig. S9B), autophagy (Fig. S9C), ER stress (Fig. S9D) as well as *SIGMAR1* expression (Fig. S9E) in astrocytes induced by methamphetamine, which is consistent with the results obtained in A172 cells transfected with human *circHIPK2* siRNA as well as that in mice microinjected with *circHIPK2* siRNA1 lentivirus.

The interaction between *MIR124-2HG* and *circHIPK2* was further confirmed by a miR affinity-isolation assay. To support the *circHIPK2*-*MIR124-2HG*-*SIGMAR1* network in our study, we examined the level of *MIR124-2HG* in astrocytes transduced with *circHIPK2* siRNA and found that knockdown of *circHIPK2* expression did not significantly affect the level of *MIR124-2HG* (Fig. S10A and B). However, the level of *MIR124-2HG* binding with *circHIPK2* was significantly decreased in the *circHIPK2* siRNA-transduced group compared with the siRNA control-treated group as determined using an affinity-isolation assay (Fig. S10C). Moreover, we examined the effect of *circHIPK2*-*MIR124-2HG* axis on the expression of *SIGMAR1* in astrocytes without/with methamphetamine. As shown in Fig. S11, knockdown of *circHIPK2* significantly inhibited the expression of *SIGMAR1* induced by *Anti-MIR124-2HG* in A172 cells or primary mouse astrocytes treated with methamphetamine. A recent study indicates that another circRNA, *circHIPK3*, acts as a sponge for *MIR124-2HG* and regulates cell proliferation.³⁵ *circHIPK3* is derived from exon 2 of the *HIPK3* gene, and it has been identified in previous reports via the deep sequencing of several human cell lines.^{31,42,43} To our knowledge, this is the first report demonstrating that knockdown of *circHIPK2* expression inhibits astrocyte activation induced by methamphetamine and LPS.

Although the present study showed that *MIR124-2HG* is regulated by *circHIPK2*, our results do not exclude the involvement of other circRNAs or molecules in the regulation of *MIR124-2HG*, either directly or indirectly. On the contrary, *circHIPK2* was not specifically targeting *MIR124-2HG*. Using starBase v2.0 software, we predicted that *circHIPK2* is able to bind other miRNAs that are involved in the regulation of autophagy-associated proteins, such as *MIR146A*, *MIR302A*, *MIR372*, *MIR373*, *MIR378A*, *MIR506* and *MIR520A*. In our study, we further examined the effect of methamphetamine on the expression of these miRNAs. As shown in Fig. S12, methamphetamine treatment significantly decreased the expression of *MIR146A*, but not *MIR372* or *MIR378A*. Notably, in primary mouse astrocytes, the levels of *Mir302a*, *Mir373*, *Mir506* and *Mir520a* were not detectable. Therefore, it remains to be elucidated whether the binding of other miRNAs to *circHIPK2* is involved in astrocyte activation. In terms of the targeting of miRNAs, it is known that one miRNA may have many targets.⁴⁴ Using TargetScan, we have predicted that, in addition to *SIGMAR1*, there are other targets for *MIR124-2HG* including *BECN1*, *RHOG*, *SNAI2*, *MAGT1* and *PTBP1*. Among these targets, only *BECN1* is involved in the regulation of autophagy. In our study, methamphetamine treatment increased the expression of *BECN1*. Consistent with a recent study showing that decreased *MIR124-2HG* expression enhances the proliferation of breast cancer cells targeting *BECN1*,⁴⁵ our current

study also indicated that transduction of cells with *Anti-MIR124-2HG* increased the expression of BECN1, as shown in Fig. S13A. Moreover, loss-of-function experiments knocked down BECN1 expression, suggesting that SIGMAR1 lies upstream of BECN1 (Fig. S13 A and B). Although we could not rule out the possibility that methamphetamine-induced autophagy was due to another target of *MIR124-2HG*-BECN1, our study provides convincing evidence that the *MIR124-2HG*-SIGMAR1 axis is involved in the autophagy induced by methamphetamine.

To date, increasing numbers of miRs have been found to be key regulators of different cellular processes, particularly those related to autophagy and ER stress. However, few studies have assessed the regulatory mechanisms of these miRs in astrocytes. *MIR124-2HG*, the most abundant brain-specific miR, regulates microglial²⁸ and astrocyte²⁹ activation. Consistent with these findings, our study showed that *MIR124-2HG* expression was decreased in astrocytes treated with methamphetamine and that *MIR124-2HG* overexpression significantly inhibited methamphetamine-induced astrocyte activation (Fig. 2A and B). To determine whether *MIR124-2HG*-mediated functional effects depend specifically on SIGMAR1 suppression, a *MIR124-2HGΔ* lentivirus construct with mutations in the sequence targeting the 3'-UTR of *SIGMAR1* was generated (Fig. S14A). Overexpression of a *MIR124-2HG*, but not the *MIR124-2HGΔ* construct with mutations in the sequence targeting the 3'-UTR of *SIGMAR1*, significantly inhibited the increased expression of SIGMAR1, GFAP and MAP1LC3B-II in astrocytes induced by methamphetamine (Fig. S14B). Consistent with this finding, microinjection of a *MIR124-2HG* lentivirus significantly inhibited the increased expression of GFAP and MAP1LC3B-II induced by methamphetamine (Fig. S15A) or LPS (Fig. S15B). However, the *MIR124-2HGΔ* construct with mutations in the sequence targeting the 3'-UTR of *SIGMAR1* failed to affect these responses. Although previous studies have indicated that *MIR124-2HG* is involved in glial activation, its detailed function in astrocyte activation and whether it participates in autophagy and ER stress remain an enigma. Our current study focused on elucidation of the role of *MIR124-2HG* in the regulation of astrocyte activation via the interplay between autophagy and ER stress. Our findings demonstrated that *MIR124-2HG* inhibits autophagy and ER stress with consequent astrocyte activation through the targeting of SIGMAR1.

Autophagy is a basic cellular process that results in the degradation of defective organelles and misfolded proteins to preserve cellular homeostasis. A previous study indicates that autophagy contributes to astrocyte activation, as evidenced by the finding that the autophagy inhibitor 3-MA decreases astrocyte activation induced by cocaine in astrocytes.⁴⁶ Surprisingly, our results demonstrated that the autophagy inducer rapamycin significantly decreased astrocyte activation, while the autophagy inhibitor 3-MA had significant inductive effects, suggesting that methamphetamine-induced autophagy inhibits astrocyte activation. To obtain more solid evidence, we further extended the study and confirmed the role of autophagy in astrocyte activation induced by LPS, as evidenced by the finding that rapamycin significantly inhibited the LPS-induced increase in GFAP expression (Fig. S16). Our findings are consistent with a previous study showing that rapamycin decreases

astrocyte activation induced by spinal cord injury⁴⁷ as well as another study demonstrating that conditioned deletion of MTOR in astrocytes with MTOR downregulation significantly ameliorates astrogliosis in the sclerotic hippocampus.⁴⁵ Controversy exists in the role of autophagy during astrocyte activation, as a recent study indicates that inhibition of autophagy results in the attenuation of astrocyte activation.⁴⁶ Whether autophagy inhibits or enhances astrocyte activation mainly depends on distinct autophagy-related signaling pathways triggered by different stimuli in specific contexts. In the current study, we provide the first demonstration of a molecular link between *circHIPK2* and autophagy. Knockdown of *circHIPK2* expression significantly decreased autophagy triggered by methamphetamine via *MIR124-2HG* and its target SIGMAR1. To the best of our knowledge, this is the first report of a role for this circRNA in the regulation of autophagy. Whether *circHIPK2* and *MIR124-2HG* are also involved in other neurodegenerative diseases is an interesting question that should be addressed in future investigations. Thus, it will be critical to determine whether *circHIPK2* and *MIR124-2HG* function in other astrocyte activation pathways and to identify the relevant substrates.

Given that ER stress induced by numerous stress stimuli, such as hypoxia, infection and nutrient depletion, triggers activation of astrocytes,^{48,46} we next examined the effect of methamphetamine on ER stress in astrocytes. The results demonstrated that exposure of astrocytes to methamphetamine induced activation of ER stress, ultimately leading to astrocyte activation. Emerging evidence indicates that ER stress plays key roles in the induction of astrocyte activation⁴⁹ and astrocyte survival.⁵⁰ Recent studies have shown that ER stress in response to psychostimulants is linked to behavioral sensitization and that the psychostimulant-induced ER stress signaling cascades are closely associated with the pathogenesis of neurodegenerative diseases.^{46,51} In the current study, we provide the first demonstration of a molecular link between *circHIPK2* and ER stress-mediated astrocyte activation. Knockdown of *circHIPK2* expression resulted in significantly decreased ER stress triggered by methamphetamine via *MIR124-2HG* and its target SIGMAR1. To the best of our knowledge, this is the first report of a role for circRNAs in the regulation of ER stress.

Our study has clarified that autophagy has an inhibitory effect on astrocyte activation, while ER stress has an inductive effect, indicating that autophagy and ER stress play distinct roles in this process. Previous studies have demonstrated a central role for ER stress in the induction of autophagy in glioma cells.^{52,53} To further clarify the relationship between ER and autophagy, we examined the effect of hypoxia (ER stress inducer) and the autophagy inhibitor 3-MA on the expression of GFAP in the same experiment. As shown in Fig. S17, pretreatment of astrocytes with 3-MA significantly inhibited the increased GFAP expression induced by hypoxia, suggesting that ER stress leads to autophagy, which then leads to astrocyte activation. In our current study, methamphetamine treatment also induced ER stress, and the ER stress inhibitor salubrinal inhibited autophagy and the activation of astrocytes induced by methamphetamine (Fig. 11A and B). However, pretreatment of astrocytes with the autophagy inducer rapamycin, but not the autophagy inhibitor 3-MA, inhibited GFAP expression induced by methamphetamine (Fig. 10C to F). While ER stress lies

upstream of autophagy, autophagy in turn responds and inhibits the ER stress as evidenced by the fact that rapamycin treatment inhibited the ER stress induced by methamphetamine (Fig. 11C and D), while the autophagy inhibitor 3-MA enhanced ER stress (Fig. 11E and F). Based on our findings, it is possible to interpret the role of autophagy as a “beneficial guardian” that inhibits ER stress through negative-feedback mechanism as well as the activation of astrocytes induced by methamphetamine. Coregulation of methamphetamine-induced astrocyte activation was found to involve autophagy and the ER stress response. Taken together, these findings suggest that autophagy and ER stress function cooperatively in the regulation of astrocyte activation.

Thus, the results of our current study reveal for the first time that *circHIPK2* regulates astrocyte activation by targeting the *MIR124-2HG-SIGMAR1* pathway via the interplay between autophagy and ER stress. Our data shed new light on the role of *circHIPK2* in astrocyte activation. Specific blockage of *circHIPK2* shows potential as a therapeutic target for inhibition of astrocyte activation in the context of drug abuse as well as for the treatment of a broad range of neuroinflammatory disorders.

Methods

Reagents

Lentiviral vectors carrying *MIR124-2HG*, *Anti-MIR124-2HG*, *circHIPK2* siRNA, *MIR124-2HGΔ* construct with a mutated sequence that does not target the 3'-UTR of *SIGMAR1* (*MIR124-2HGΔ*) and an adenoviral vector carrying mRFP-GFP-MAP1LC3B (HB-AP2100001) were purchased from HanBio (Shanghai, China). Human *circHIPK2* siRNA based on the sequence 5'-GUCCAGAUUUACAGGUAUTT-3' was purchased from GenePharma (Shanghai, China) and purified by HPLC. Scrambled nontargeting siRNA (GenePharma, Shanghai, China) with the following sequence was used as negative control: 5'-UUCUCCGAACGUGUCACGUTT-3'. For the lentiviral vectors carrying the construct with a mutated *MIR124-2HG* (*MIR124-2HGΔ*, Table 1D) that does not target the 3'-UTR of *SIGMAR1*, the *MIR124-2HG* sequence (UAAGGCA) targeting the 3'-UTR of *SIGMAR1* was changed to UCGACAC, which was obtained from HanBio. Methamphetamine was obtained from the National Institute for the Control of Pharmaceutical and Biological Products. *Control* siRNA (sc-37007), human *SIGMAR1/OPRS1* siRNA (sc-42250), LPS (L2630), rapamycin (R0395) and 3-MA (M9281) were purchased from Sigma-Aldrich. Salubrinal (SML0951) was from Sigma-Aldrich.

Animals

Sigmar1 KO mice were obtained from the Laboratory Animal Center of University of Science and Technology of China (Hefei, China); these mice were backcrossed for 10 generations to a C57BL/6N inbred background. C57BL/6N mice (male, 6 to 8 wk old) were purchased from the Comparative Medicine Center, Yangzhou University (Yangzhou, China). All animals were housed at a constant temperature and humidity with a 12 h light:12 h dark cycle, with lights on at 07:00. Food and water were available *ad libitum*. The animals were deeply

anesthetized by an overdose of isoflurane, followed by pneumothorax, before perfusion. All animal procedures were performed according to protocols approved by the Institutional Animal Care and Use Committee of the Medical School, Southeast University.

Cell cultures

Primary mouse astrocytes were obtained from postnatal (P1 to P2) C57BL/6N mice. Whole brains were removed from the mice and were then dissected and mechanically dissociated using gauze to remove membranes and large blood vessels. Next, the dissected brain cortices were placed in medium supplemented with phosphate-buffered serum (PBS; 2.96 mM Na₂HPO₄·7H₂O, 1.05 mM KH₂PO₄, 155.17 mM NaCl, pH 7.4), and the brain tissues were digested with trypsin-EDTA (Gibco, 25200056). Subsequently, the cells were plated on poly-L-lysine precoated cell culture flasks containing Dulbecco's modified Eagle's medium (DMEM; Corning, 32016001) supplemented with fetal bovine serum (10% v/v) and penicillin/streptomycin (1% v/v). The cultures were maintained in a humidified chamber (37 °C, 5% CO₂ incubator). After 7 to 10 days, the astrocytes were harvested by trypsinization.

The human astrocytoma cell line A172 (ATCC[®] CRL1620[™]) was obtained from the China Center for Type Culture Collection, routinely maintained in DMEM (10% fetal bovine serum and 1% penicillin/streptomycin) and incubated at 37 °C and 5% CO₂.

Luciferase activity assays

The 3'-UTR of the 945-base pair human *SIGMAR1* gene containing the putative *MIR124-2HG* target site was PCR-amplified from human genomic DNA using forward (5'-GCGCTCGAGCTCACCACCTACCTCT-3') and reverse (5'-AATGCGGCCGCGAACAGATCAACAAATCT-3') primers, and the DNA fragment was cloned into the XhoI and NotI sites on the 3'-end of the *luc2* gene in a pmiR-RB-REPORT[™] vector (RiboBio). For the pmiR-RB-*SIGMAR1*-3'-UTR-*MIR124-2HG*-target-mutant vector, the *MIR124-2HG* target site (TGCCCTTA) within the *SIGMAR1* 3'-UTR was changed to ACGGAAT by PCR mutagenesis with the primers *SIGMAR1-MIR124-2HGT-F* (5'-TCACCATAACGGAATCCCCATTC-TACTCCCT-3') and *SIGMAR1-MIR124-2HGT-R* (5'-AATGGGAATTCGGTTATGGTGAGGACAGGGGA-3'). Briefly, HEK293T cells were transfected with a *MIR124-2HG* overexpression pLV-[*hsa-MIR124-2HG*] vector (RiboBio) and a target plasmid, pmiR-RB-*SIGMAR1*-3'-UTR or pmiR-RB-*SIGMAR1*-3'-UTR-*MIR124-2HG*-target-mutant, at a molar ratio of 50:1. A miR control pLV-[*MIR control*] plasmid was used as a negative control. Luciferase activity was determined 24 h post-transfection, and the reporter assay was performed following the manufacturer's protocol (Promega, E2920). Renilla luciferase activity was normalized to firefly luciferase activity and expressed as a percentage of the control (n>3, determined from 5 wells each sample).

Western blot analysis

Proteins were extracted in RIPA lysis buffer (Beyotime, P0013B). Proteins were separated by sodium dodecyl sulfate-polyacrylamide gel electrophoresis (12%) and electrophoretically transferred onto polyvinylidene fluoride membranes. The membranes were blocked with 5% nonfat dry milk in Tris-buffered saline with Tween-20 (Aladdin, T104863), probed with antibodies overnight at 4°C and then incubated with a horseradish peroxidase-conjugated goat anti-mouse (ZSGB-BIO, ZB5305) or rabbit (ZSGB-BIO, ZB5301) IgG secondary antibody (1:2000). The antibodies used were as follows: anti-GFAP (G3893), obtained from Sigma-Aldrich; anti-SIGMAR1/OPRS1 (sc137075), anti-ACTB/ β -actin (sc1616), anti-EIF2AK3 (sc13073), anti-ERN1 (sc20790), anti-ATG5 (sc33210) and anti-ATF6 (sc166659), purchased from Santa Cruz Biotechnology; anti-SQSTM1 (18420), anti-BECN1 (11306), anti-MAP1LC3B (14600), anti-GAPDH (60004) and anti-DDIT3 (15204), acquired from Proteintech; and anti-EIF2S1 (5324s), obtained from Cell Signaling Technology. Detection was performed using a MicroChemi 4.2[®] (DNR, Israel) digital image scanner. Band intensity was quantified using ImageJ software (NIH).

Real-time PCR

Total RNA was isolated from cells and subjected to reverse transcription using a PrimeScript RT Master Mix Kit (TaKaRa, RR036). Real-time PCR was performed by StepOne[™] Real-Time PCR System (Life Technologies, 4376357, Singapore) using the following primers: human divergent *circHIPK2* (forward primer: 5'-CTGTGTGCTCCACCTACTTG-3'; reverse primer: 5'-TACCCAGTCATGTCCCAGTTG-3'), human *GAPDH* (forward primer: 5'-ACCATCTTCCAGGAGCGAGAT-3'; reverse primer: 5'-GGGCAGAGATGATGACCCTTT-3'), mouse divergent *circHIPK2* (forward primer: 5'-GACAACCGTACCGAGTGAAG-3'; reverse primer: 5'-GTGTGAGGGGGA-GAAAACCTTGC-3'), mouse *circHIPK2* convergent primer (forward: 5'-GCAAGTTTTCTCCCCTCACAC-3'; reverse: 5'-CTTCACTCGGTACGGTTGTC-3'), mouse divergent *Gapdh* (forward primer: 5'-AGGTCGGTGTGAACGGATTTG-3'; reverse primer: 5'-GGGGTCGTTGATGGCAACA-3') and mouse *Gapdh* convergent primer (forward: 5'-AGGTCGGTGTGAACGGATTTG-3'; reverse: 5'-GGGGTCGTTGATGGCAACA-3'). Relative quantification was performed using TaKaRa SYBR[®] Premix Taq[™] (TbI RNase H Plus; TaKaRa, RR420). The sequences for knockdown of *circHIPK2* expression: human *circHIPK2* siRNA: 5'-GUCCAGAUUUACAGGUAUTT-3'; mouse *circHIPK2* siRNA 1: 5'-UACCGGUAUGGCCUCAUTT-3'; mouse *circHIPK2* siRNA 2: 5'-UCCAGUAUCUACCGGUAUGTT-3'. Specific primers and probes for mature *MIR124-2HG* and *RNU6-6P/RNU6B* were obtained from RiboBio. All reactions were run in triplicate. The amount of *MIR124-2HG* was determined by normalizing to the level of *RNU6-6P* relative to that in the control as previously reported.⁵⁴

Fluorescence in situ hybridization (FISH)

According to our previous study,⁵⁵ primary mouse astrocytes cultured in coverslips were fixed with 4% paraformaldehyde for

20 min and incubated in PBS overnight at 4°C followed by the detection of *circHIPK2* and *MIR124-2HG* expression. The cells were permeabilized with 0.25% Triton X-100 (Aladdin, T109027) in PBS for 15 min, prehybridized in hybridization buffer (50% formamide, 10 mM Tris-HCl, pH 8.0, 200 μ g/ml yeast tRNA [Sigma-Aldrich, 15401-011], 1X Denhardt solution [Sigma-Aldrich, 30915], 600 mM NaCl, 0.25% SDS [Invitrogen, 15553-035], 1 mM EDTA, 10% dextran sulfate [Sigma-Aldrich, D8906]) for 1 h at 37°C. Then, the coverslips were heated to 65°C for 5 min in hybridization buffer containing 2 nM of a commercially available digoxigenin-labeled *MIR124-2HG* probe (Exiqon, Table 1E) and 500 nM of a commercially available biotin-labeled *circHIPK2* probe (Invitrogen) hybridization occurred at 37°C overnight. The next day, the coverslips were washed 3 times in 2X SSC (10% v/v 20X SSC [Invitrogen, 15557] in DEPC-treated water [Vetec, V900882]) and twice in 0.2X SSC (10% v/v 2X SSC in DEPC-treated water) at 42°C and then blocked with 1% BSA (Biosharp, BS043D), 3% normal goat serum (ZSGB-BIO, ZLI-0956) in PBS for 1 h at room temperature. They were then incubated with a horseradish peroxidase-conjugated anti-digoxigenin antibody (1:200; Roche Diagnostics GmbH, 11207733910) and FITC-streptavidin (1:200; Life Technology, 434311) overnight at 4°C. After the coverslips were washed 3 times with TBS (0.1 M Tris, 0.308 M NaCl, pH 7.4), they were incubated with a TSA Cy5 kit (PerkinElmer, NEL766B001KT) for 10 min at room temperature. Then, the coverslips were washed twice with PBS and mounted with Prolong gold anti-fade reagent containing DAPI (SouthernBiotech, 0100-20). In the FISH experiments, the specificity of the *circHIPK2* and *MIR124-2HG* signal was confirmed via comparison with a scrambled control. Unlike the *circHIPK2* and *MIR124-2HG* probe, the scrambled probe showed no signal in primary mouse astrocytes.

Affinity-isolation assay with biotinylated *MIR124-2HG*

A total of 2×10^6 HEK 293T cells were seeded the day before transfection. On the following day, the cells were transfected with 3'-end biotinylated *MIR124-2HG* or *MIR124-2HG Δ* at a final concentration of 50 nM for 36 h. Then, the cells were washed with PBS, briefly vortexed and incubated in lysis buffer (20 mM Tris, pH 7.5, 200 mM NaCl, 2.5 mM MgCl₂, 0.05% Igepal [Sigma, I3021], 60 U/ml Superase-In [Ambion, AM2694], 1 mM DTT [Sigma, 43816] and protease inhibitors [Biotool, B14001]) on ice for 10 min. Lysates were precleared by centrifugation, and 50 μ l aliquots of the samples were prepared for input. The remaining lysates were incubated with M-280 streptavidin magnetic beads (Invitrogen, 11205D). The beads were coated with yeast tRNA in advance to prevent the nonspecific binding of RNA and protein complexes. The beads were incubated at 4°C for 2.5 h and were then washed twice with ice-cold lysis buffer, twice with low-salt buffer (0.1% SDS, 1% Triton X-100, 2 mM EDTA, 20 mM Tris-HCl, pH 8.0, 150 mM NaCl) and once with high-salt buffer (0.1% SDS, 1% Triton X-100, 2 mM EDTA, 20 mM Tris-HCl, pH 8.0, 500 mM NaCl). The bound RNAs were purified using Trizol (TaKaRa, 9109) for measurement of *circHIPK2* levels. The biotinylated *MIR124-2HG* at the 3'-end was synthesized by GenePharma (Shanghai, China), and its sequence was 5'-UAAGGCACGCGGUGAAUGCC-3'. The

*MIR124-2HG*Δ sequence was 5'-UCGACACCGCGGU-GAAUGCC-3' and also biotinylated at the 3'-end.

Affinity-isolation assay with DNA probe

The biotinylated DNA probe complementary to *circHIPK2* was synthesized and dissolved in 500 μl of wash/binding buffer (0.5 M NaCl, 20 mM Tris-HCl, pH 7.5, 1 mM EDTA). The probes were incubated with streptavidin-coated magnetic beads (Sigma, 08014) at 25°C for 2 h to generate probe-coated magnetic beads. Cardiomyocyte lysates were incubated with probe-coated beads, and after washing with the wash/binding buffer, the RNA complexes bound to the beads were eluted and extracted for real-time PCR. The following primer sequences were used: *circHIPK2* affinity-isolation probe, AAAACATGTGAGGCCATACCTG-TAATATCTGGACT; and random affinity-isolation probe, AAACAGTACTGGTGTGTAGTACGAGCTGAAGCTAC.

Transduction of astrocytes with lentivirus

Astrocytes were transduced with *MIR control*, *MIR124-2HG*, *Anti-MIR control*, *Anti-MIR124-2HG*, *circ control* siRNA and *circHIPK2* siRNA lentivirus with multiplicity of infection of 0.5 (primary mouse astrocytes) or 10 (A172 cells), followed by gentle swirling, incubation and replacement of fresh feed medium.

Microinjection of Anti-MIR124-2HG or circHIPK2 siRNA lentivirus

The hippocampi of 8-wk-old C57BL/6 mice were microinjected bilaterally with an *Anti-MIR control*-RFP, *Anti-MIR124-2HG*-RFP, *circ control* siRNA-GFP or *circHIPK2* siRNA-GFP lentivirus (2 μl of 10⁹ viral genomes μl⁻¹, HanBio) using the following microinjection coordinates: 2.06 mm behind the bregma and ± 1.5 mm lateral from the sagittal midline at a depth of 2 mm from skull surface. To evaluate the effect of *Anti-MIR124-2HG* on astrocyte activation in WT and *sigmar1* KO mice, 12 mice (n = 6/group; male) were perfused and sectioned 2 wk after lentivirus microinjection, followed by GFAP staining to assess astrocyte activation. To evaluate the effect of *circHIPK2* siRNA on methamphetamine/LPS-induced astrocyte activation, 18 mice were divided into 3 groups (n = 6/group; male) 2 wk after lentivirus microinjection and treated with saline, methamphetamine (30 mg/kg, injected every 2 h for a total of 4 times, intraperitoneally [i.p.]) for 24 h or LPS (20 mg/kg, i.p.) for 4 h. Then, the animals were perfused and sectioned, followed by GFAP staining to assess astrocyte activation.

Immunostaining and image analysis

As described in our previous study,⁵⁵ the sections encompassing the entire hippocampus were cut into 35 μm slices with a cryostat. Then, the sections were incubated with 0.3% Triton X-100 in PBS for 15 min and blocked with 10% normal goat serum in 0.3% Triton X-100 for 1 h at room temperature. Next, the sections were incubated with a mouse anti-GFAP antibody (Sigma-Aldrich, G3893) overnight at 4°C. On the following day, the sections were washed and incubated with Alexa Fluor 488-conjugated anti-mouse IgG (1:250; Invitrogen, A11001) or Alexa

Fluor 594 goat anti-mouse IgG (1:250; Invitrogen, A11005) for 1 h to detect GFAP. After a final washing step with PBS, the sections were mounted onto glass slides, and ProLong gold Antifade reagent containing DAPI (SouthernBiotech, 0100-20) was applied for visualization of nuclei. Immunofluorescence images were captured by microscopy (Olympus DP73, Olympus, Tokyo, Japan). Average intensities of GFAP were calculated using ImageJ by sampling of a 28 × 28 pixel area, and 36 images were captured from 6 consecutive sections. The values were reported as the average intensity above the background ± SD.

Transmission electron microscopy

Cells were cultured in 24-well plates and treated with 100 μM methamphetamine. After incubation of the cells with methamphetamine for 24 h, the treated cells from each sample were harvested in a 1.5 ml microcentrifuge tube. The cells were washed once with cold PBS and fixed in a mixture of 2% glutaraldehyde and 2% formaldehyde in 0.1 M sodium cacodylate buffer (pH 7.4) at 4°C overnight. Then, they were washed 4 times in 0.1 M sodium cacodylate buffer (pH 7.4) containing 264 mM sucrose (Sinopharm, 10021418) before being transferred to 1% osmium tetroxide in 0.1 M sodium cacodylate (pH 7.4) for 2 h. The cells were then washed 3 times in double distilled H₂O and stained in 2% aqueous uranyl acetate for 2 h. Next, they were dehydrated in an ethanol series, infiltrated in propylene oxide (Aladdin, R101941) 2 times and embedded in Epon 812 (SPI Science, 90529-77-4). Ultrathin sections (90-nm thick) were cut using a Leica EM UC7 ultramicrotome (Ser. No: 595915, Austria) with a diamond knife. Grids were post-stained with 2% saturated uranyl acetate in 50% ethanol and 1% lead citrate (pH 12) and examined using an H-7650 electron microscope (Hitachi, Tokyo, Japan), and images were captured with a Ganton 830 digital camera.

Tandem fluorescent-mRFP-GFP-MAP1LC3B-adenovirus transduction of A172 cells

A172 cells were transfected with a tandem fluorescent-mRFP-GFP-MAP1LC3B-adenovirus (HanBio, HB-AP2100001) that expresses a specific marker of autophagosome formation to detect autophagy, according to the manufacturer's instructions.⁵⁶ Five fields were chosen from 3 different cell preparations. GFP- and mRFP-expressing spots, which were indicated by fluorescent puncta and DAPI-stained nuclei were counted manually. The number of spots per cell was determined by dividing the total number of spots by the number of nuclei in each field.

Rapamycin administration

Rapamycin (LC Laboratories, R-5000) was dissolved in DMSO (25 mg/ml). For animal injections, the stock solution was diluted immediately before i.p. injection with 100 μl water containing 5% polyethylene glycol 400 (Damas-β, 41713B) and 5% Tween-80 (Aladdin, T104866). Mice received rapamycin (5 mg/kg, i.p.) 24 h before the last methamphetamine injection, and control mice received the drug vehicle.

Statistical analyses

Statistical analysis was performed using the Student *t* test or one-way analysis of variance (ANOVA) followed by the Holm-Sidak test (SigmaPlot 11.0). The tests used are indicated in the figure legends. The ANOVA results were considered significant at a $P < 0.05$.

Abbreviations

3-MA	3-methyladenine
ACTB	actin β
ATG5	autophagy-related 5
BBB	blood-brain barrier
BECN1	Beclin 1, autophagy related
CNS	central nervous system
circRNA	circular RNA
<i>circHIPK2</i>	circular RNA <i>HIPK2</i>
DAPI	4',6-diamidino-2-phenylindole
DDIT3	DNA damage inducible transcript 3
ER	endoplasmic reticulum
EIF2AK3	eukaryotic translation initiation factor 2 α kinase 3
EIF2S1	eukaryotic translation initiation factor 2 subunit α
ERN1	endoplasmic reticulum to nucleus signaling 1
FISH	fluorescence <i>in situ</i> hybridization
GAPDH	glyceraldehyde-3-phosphate dehydrogenase
GFAP	glial fibrillary acidic protein
KO	knockout
LPS	lipopolysaccharide
LV	lentivirus
MAP1LC3B	microtubule-associated protein 1 light chain 3 β
Meth	methamphetamine
<i>MIR124-2HG</i>	MIR124-2 host gene
miRNAs	microRNAs
MTOR	mechanistic target of rapamycin (serine/threonine kinase)
OE	overexpression
SIGMAR1/OPRS1	sigma non-opioid intracellular receptor 1
PCR	polymerase chain reaction
SQSTM1	sequestosome 1
UTR	untranslated region
WT	wild type

Disclosure of potential conflicts of interest

The authors declare that there are no competing financial interests.

Acknowledgments

This work was supported by grants from the National Natural Science Foundation of China (No. 81322048, No. 81673410 and No. 81603090), the Jiangsu Specially Appointed Professor and the Major State Basic Research Development Program of China (973 Program) (2013CB733800 and 2013CB733803).

References

- Shirakawa H, Sakimoto S, Nakao K, Sugishita A, Konno M, Iida S, Kusano A, Hashimoto E, Nakagawa T, Kaneko S. Transient receptor potential canonical 3 (TRPC3) mediates thrombin-induced astrocyte activation and upregulates its own expression in cortical astrocytes. *J Neurosci*. 2010;30(39):13116-29. doi:10.1523/JNEUROSCI.1890-10.2010. PMID:20881130
- Williams A, Piaton G, Lubetzki C. Astrocytes—friends or foes in multiple sclerosis? *Glia*. 2007;55(13):1300-12. doi:10.1002/glia.20546. PMID:17626262
- Iadecola C, Nedergaard M. Glial regulation of the cerebral microvasculature. *Nat Neurosci*. 2007;10(11):1369-76. doi:10.1038/nn2003. PMID:17965657
- Dong Y, Benveniste EN. Immune function of astrocytes. *Glia*. 2001;36(2):180-90. doi:10.1002/glia.1107. PMID:11596126
- Sofroniew MV. Molecular dissection of reactive astrogliosis and glial scar formation. *Trends Neurosci*. 2009;32(12):638-47. doi:10.1016/j.tins.2009.08.002. PMID:19782411
- Nair A, Frederick TJ, Miller SD. Astrocytes in multiple sclerosis: A product of their environment. *Cell Mol Life Sci*. 2008;65(17):2702-20. doi:10.1007/s00018-008-8059-5. PMID:18516496
- Yan Y, Ding X, Li K, Ciric B, Wu S, Xu H, Gran B, Rostami A, Zhang GX. CNS-specific therapy for ongoing EAE by silencing IL-17 pathway in astrocytes. *Mol Ther*. 2012;20(7):1338-48. doi:10.1038/mt.2012.12. PMID:22434134
- Rossi DJ, Brady JD, Mohr C. Astrocyte metabolism and signaling during brain ischemia. *Nat Neurosci*. 2007;10(11):1377-86. doi:10.1038/nn2004. PMID:17965658
- Shao W, Zhang SZ, Tang M, Zhang XH, Zhou Z, Yin YQ, Zhou QB, Huang YY, Liu YJ, Wawrousek E, et al. Suppression of neuroinflammation by astrocytic dopamine D2 receptors via alphaB-crystallin. *Nature*. 2013;494(7435):90-4. doi:10.1038/nature11748. PMID:23242137
- Halliday GM, Stevens CH. Glia: Initiators and progressors of pathology in Parkinson's disease. *Mov Disord*. 2011;26(1):6-17. doi:10.1002/mds.23455. PMID:21322014
- Verkhatsky A, Olabarria M, Noristani HN, Yeh CY, Rodriguez JJ. Astrocytes in Alzheimer's disease. *Neurotherapeutics*. 2010;7(4):399-412. doi:10.1016/j.nurt.2010.05.017. PMID:20880504
- Rodriguez JJ, Olabarria M, Chvatal A, Verkhatsky A. Astroglia in dementia and Alzheimer's disease. *Cell Death Differ*. 2009;16(3):378-85. doi:10.1038/cdd.2008.172. PMID:19057621
- Zhang Y, Zhu T, Zhang X, Chao J, Hu G, Yao H. Role of high-mobility group box 1 in methamphetamine-induced activation and migration of astrocytes. *J Neuroinflammation*. 2015;12:156. doi:10.1186/s12974-015-0374-9. PMID:26337661
- Lau JW, Senok S, Stadlin A. Methamphetamine-induced oxidative stress in cultured mouse astrocytes. *Ann N Y Acad Sci*. 2000;914:146-56. doi:10.1111/j.1749-6632.2000.tb05192.x. PMID:11085317
- Clark KH, Wiley CA, Bradberry CW. Psychostimulant abuse and neuroinflammation: Emerging evidence of their interconnection. *Neurotox Res*. 2013;23(2):174-88. doi:10.1007/s12640-012-9334-7. PMID:22714667
- Pu C, Vorhees CV. Developmental dissociation of methamphetamine-induced depletion of dopaminergic terminals and astrocyte reaction in rat striatum. *Brain Res Dev Brain Res*. 1993;72(2):325-8. doi:10.1016/0165-3806(93)90201-K. PMID:8097974
- Robson MJ, Turner RC, Naser ZJ, McCurdy CR, O'Callaghan JP, Huber JD, Matsumoto RR. SN79, a sigma receptor antagonist, attenuates methamphetamine-induced astrogliosis through a blockade of OSMR/gp130 signaling and STAT3 phosphorylation. *Exp Neurol*. 2014;254:180-9. doi:10.1016/j.expneurol.2014.01.020. PMID:24508558
- Shah A, Kumar S, Simon SD, Singh DP, Kumar A. HIV gp120- and methamphetamine-mediated oxidative stress induces astrocyte apoptosis via cytochrome P450 2E1. *Cell Death Dis*. 2013;4:e850. doi:10.1038/cddis.2013.374. PMID:24113184
- Shah A, Silverstein PS, Singh DP, Kumar A. Involvement of metabolic glutamate receptor 5, AKT/PI3K signaling and NF-kappaB

- pathway in methamphetamine-mediated increase in IL-6 and IL-8 expression in astrocytes. *J Neuroinflammation*. 2012;9:52. doi:10.1186/1742-2094-9-52. PMID:22420994
- [20] Colombo E, Farina C. Astrocytes: Key regulators of neuroinflammation. *Trends Immunol*. 2016;37(9):608-20. doi:10.1016/j.it.2016.06.006. PMID:27443914
- [21] Argaw AT, Asp L, Zhang J, Navrazhina K, Pham T, Mariani JN, Mahase S, Dutta DJ, Seto J, Kramer EG, et al. Astrocyte-derived VEGF-A drives blood-brain barrier disruption in CNS inflammatory disease. *J Clin Invest*. 2012;122(7):2454-68. doi:10.1172/JCI60842. PMID:22653056
- [22] Sharkey J, Glen KA, Wolfe S, Kuhar MJ. Cocaine binding at sigma receptors. *Eur J Pharmacol*. 1988;149(1-2):171-4. doi:0014-2999(88)90058-1. PMID:2840298
- [23] Su TP, London ED, Jaffe JH. Steroid binding at sigma receptors suggests a link between endocrine, nervous, and immune systems. *Science*. 1988;240(4849):219-21. doi:10.1126/science.2832949. PMID:2832949
- [24] Lim LP, Lau NC, Garrett-Engele P, Grimson A, Schelter JM, Castle J, Bartel DP, Linsley PS, Johnson JM. Microarray analysis shows that some microRNAs downregulate large numbers of target mRNAs. *Nature*. 2005;433(7027):769-73. doi:10.1038/nature03315. PMID:15685193
- [25] Cheng LC, Pastrana E, Tavazoie M, Doetsch F. miR-124 regulates adult neurogenesis in the subventricular zone stem cell niche. *Nat Neurosci*. 2009;12(4):399-408. doi:10.1038/nn.2294. PMID:19287386
- [26] Makeyev EV, Zhang J, Carrasco MA, Maniatis T. The MicroRNA miR-124 promotes neuronal differentiation by triggering brain-specific alternative pre-mRNA splicing. *Mol Cell*. 2007;27(3):435-48. doi:10.1016/j.molcel.2007.07.015. PMID:17679093
- [27] Yu JY, Chung KH, Deo M, Thompson RC, Turner DL. MicroRNA miR-124 regulates neurite outgrowth during neuronal differentiation. *Exp Cell Res*. 2008;314(14):2618-33. doi:10.1016/j.yexcr.2008.06.002. PMID:18619591
- [28] Ponomarev ED, Veremeyko T, Barteneva N, Krichevsky AM, Weiner HL. MicroRNA-124 promotes microglia quiescence and suppresses EAE by deactivating macrophages via the C/EBP-alpha-PU.1 pathway. *Nat Med*. 2011;17(1):64-70. doi:10.1038/nm.2266. PMID:21131957
- [29] Hamzei Taj S, Kho W, Riou A, Wiedermann D, Hoehn M. MiRNA-124 induces neuroprotection and functional improvement after focal cerebral ischemia. *Biomaterials*. 2016;91:151-65. doi:10.1016/j.biomaterials.2016.03.025. PMID:27031810
- [30] Jeck WR, Sharpless NE. Detecting and characterizing circular RNAs. *Nat Biotechnol*. 2014;32(5):453-61. doi:10.1038/nbt.2890. PMID:24811520
- [31] Memczak S, Jens M, Elefsinioti A, Torti F, Krueger J, Rybak A, Maier L, Mackowiak SD, Gregersen LH, Munschauer M, et al. Circular RNAs are a large class of animal RNAs with regulatory potency. *Nature*. 2013;495(7441):333-8. doi:10.1038/nature11928. PMID:23446348
- [32] Li X, Wu Q, Xie Y, Ding Y, Du WW, Sdiri M, Yang BB. Ergosterol purified from medicinal mushroom *Amauroderma rude* inhibits cancer growth in vitro and in vivo by up-regulating multiple tumor suppressors. *Oncotarget*. 2015;6(19):17832-46. doi:10.18632/oncotarget.4026. PMID:26098777
- [33] Boeckel JN, Jae N, Heumuller AW, Chen W, Boon RA, Stellos K, Zeiher AM, John D, Uchida S, Dimmeler S. Identification and characterization of hypoxia-regulated endothelial circular RNA. *Circ Res*. 2015;117(10):884-90. doi:10.1161/CIRCRESAHA.115.306319. PMID:26377962
- [34] Yin TP, Cai L, Xing Y, Yu J, Li XJ, Mei RF, Ding ZT. Alkaloids with antioxidant activities from *Aconitum handelianum*. *J Asian Nat Prod Res*. 2016;18(6):603-10. doi:10.1080/10286020.2015.1114473. PMID:26744060
- [35] Zheng Q, Bao C, Guo W, Li S, Chen J, Chen B, Luo Y, Lyu D, Li Y, Shi G, et al. Circular RNA profiling reveals an abundant circHIPK3 that regulates cell growth by sponging multiple miRNAs. *Nat Commun*. 2016;7:11215. doi:10.1038/ncomms11215. PMID:27050392
- [36] Du WW, Yang W, Chen Y, Wu ZK, Foster FS, Yang Z, Li X, Yang BB. Foxo3 circular RNA promotes cardiac senescence by modulating multiple factors associated with stress and senescence responses. *Eur Heart J*. 2016;38(18):1402-12. doi:10.1093/eurheartj/ehw001. PMID:26873092
- [37] Wang K, Long B, Liu F, Wang JX, Liu CY, Zhao B, Zhou LY, Sun T, Wang M, Yu T, et al. A circular RNA protects the heart from pathological hypertrophy and heart failure by targeting miR-223. *Eur heart J*. 2016;37(33):2602-11. doi:10.1093/eurheartj/ehv713. PMID:26802132
- [38] Klionsky DJ, Cuervo AM, Seglen PO. Methods for monitoring autophagy from yeast to human. *Autophagy*. 2007;3(3):181-206. doi:10.4161/auto.3678. PMID:17224625
- [39] Kroemer G, Galluzzi L, Vandenabeele P, Abrams J, Alnemri ES, Baehrecke EH, Blagosklonny MV, El-Deiry WS, Golstein P, Green DR, et al. Classification of cell death: Recommendations of the nomenclature committee on cell death 2009. *Cell Death Differ*. 2009;16(1):3-11. doi:10.1038/cdd.2008.150. PMID:18846107
- [40] Kitamura O, Takeichi T, Wang EL, Tokunaga I, Ishigami A, Kubo S. Microglial and astrocytic changes in the striatum of methamphetamine abusers. *Leg Med (Tokyo)*. 2010;12(2):57-62. doi:10.1016/j.legalmed.2009.11.001. PMID:20110187
- [41] Deng B, Zhang Y, Zhang S, Wen F, Miao Y, Guo K. MicroRNA-142-3p inhibits cell proliferation and invasion of cervical cancer cells by targeting FZD7. *Tumour Biol*. 2015;36(10):8065-73. doi:10.1007/s13277-015-3483-2. PMID:25976503
- [42] Jeck WR, Sorrentino JA, Wang K, Slevin MK, Burd CE, Liu J, Marzluff WF, Sharpless NE. Circular RNAs are abundant, conserved, and associated with ALU repeats. *RNA*. 2013;19(2):141-57. doi:10.1261/rna.035667.112. PMID:23249747
- [43] Salzman J, Chen RE, Olsen MN, Wang PL, Brown PO. Cell-type specific features of circular RNA expression. *PLoS Genet*. 2013;9(9):e1003777. doi:10.1371/journal.pgen.1003777. PMID:24039610
- [44] Hammond SM. An overview of microRNAs. *Adv Drug Deliv Rev*. 2015;87:3-14. doi:10.1016/j.addr.2015.05.001. PMID:25979468
- [45] Zhang F, Wang B, Long H, Yu J, Li F, Hou H, Yang Q. Decreased miR-124-3p expression prompted breast cancer cell progression mainly by targeting beclin-1. *Clin Lab*. 2016;62(6):1139-45. PMID:27468577
- [46] Cai Y, Arikath J, Yang L, Guo ML, Periyasamy P, Buch S. Interplay of endoplasmic reticulum stress and autophagy in neurodegenerative disorders. *Autophagy*. 2016;12(2):225-44. doi:10.1080/15548627.2015.1121360. PMID:26902584
- [47] Goldshmit Y, Kanner S, Zacs M, Frisca F, Pinto AR, Currie PD, Pinkas-Kramarski R. Rapamycin increases neuronal survival, reduces inflammation and astrocyte proliferation after spinal cord injury. *Mol Cell Neurosci*. 2015;68:82-91. doi:10.1016/j.mcn.2015.04.006. PMID:25936601
- [48] Fan Y, He JJ. HIV-1 Tat induces unfolded protein response and endoplasmic reticulum stress in astrocytes and causes neurotoxicity through glial fibrillary acidic protein (GFAP) activation and aggregation. *J Biol Chem*. 2016;291(43):22819-29. doi:10.1074/jbc.M116.731828. PMID:27609520
- [49] Klionsky DJ, Abdelmohsen K, Abe A, Abedin MJ, Abeliovich H, Acevedo Arozana A, Adachi H, Adams CM, Adams PD, Adeli K, et al. Guidelines for the use and interpretation of assays for monitoring autophagy (3rd edition). *Autophagy*. 2016;12(1):1-222. doi:10.1080/15548627.2015.1100356. PMID:26799652
- [50] Leask A. CCN6: A modulator of breast cancer progression. *J Cell Commun Signal*. 2016;10(2):163-4. doi:10.1007/s12079-016-0321-2. PMID:27086280
- [51] Go BS, Kim J, Yang JH, Choe ES. Psychostimulant-induced endoplasmic reticulum stress and neurodegeneration. *Mol Neurobiol*. 2016;54(6):4041-48. doi:10.1007/s12035-016-9969-0. PMID:27314686
- [52] Ciechomska IA, Kaminska B. ER stress and autophagy contribute to CsA-induced death of malignant glioma cells. *Autophagy*. 2012;8(10):1526-8. doi:10.4161/auto.21155. PMID:22910018
- [53] Salazar M, Carracedo A, Salanueva IJ, Hernandez-Tiedra S, Lorente M, Egia A, Vazquez P, Blazquez C, Torres S, Garcia S, et al. Cannabinoid action induces autophagy-mediated cell death through stimulation of ER stress in human glioma cells. *J Clin Invest*. 2009;119(5):1359-72. doi:10.1172/JCI37948. PMID:19425170
- [54] Hu G, Zhou R, Liu J, Gong AY, Chen XM. MicroRNA-98 and let-7 regulate expression of suppressor of cytokine signaling 4 in

- biliary epithelial cells in response to *Cryptosporidium parvum* infection. *J Infect Dis.* 2010;202(1):125-35. doi:10.1086/653212. PMID:20486857
- [55] Yao H, Ma R, Yang L, Hu G, Chen X, Duan M, Kook Y, Niu F, Liao K, Fu M, et al. MiR-9 promotes microglial activation by targeting MCPIP1. *Nat Commun.* 2014;5:4386. doi:10.1038/ncomms5386. PMID:25019481
- [56] Hariharan N, Zhai P, Sadoshima J. Oxidative stress stimulates autophagic flux during ischemia/reperfusion. *Antioxid Redox Signal.* 2011;14(11):2179-90. doi:10.1089/ars.2010.3488. PMID:20812860